LONG, T., WANG, S., CAO, W., REN, P., HE, M. and FERNANDEZ, C. 2022. Collaborative state estimation of lithium-ion battery based on multi-time scale low-pass filter forgetting factor recursive least squares - double extended Kalman filtering algorithm. *International journal of circuit theory and applications* [online], 50(6), pages 2108-2127. Available from: https://doi.org/10.1002/cta.3250

Collaborative state estimation of lithium-ion battery based on multi-time scale low-pass filter forgetting factor recursive least squares - double extended Kalman filtering algorithm.

LONG, T., WANG, S., CAO, W., REN, P., HE, M. and FERNANDEZ, C.

2022

International Journal of Circuit Theory and Applications

Collaborative state estimation of lithium-ion battery based on multi-time scale low-pass filter forgetting factor recursive least squares - double extended Kalman filtering algorithm

Journal:	*International Journal of Circuit Theory and Applications*
Manuscript ID	CTA-21-0826.R1
Wiley - Manuscript type:	Original Article
Date Submitted by the Author:	13-Jan-2022
Complete List of Authors:	Long, Tao; Southwest University of Science and Technology Wang, Shunli ; Southwest University of Science and Technology Cao, Wen; Southwest University of Science and Technology Pu, Ren; Southwest University of Science and Technology He, Mingfang; Southwest University of Science and Technology Fernandez, Carlos; Robert Gordon University
Keyword:	Low pass filter, Second-order RC model, forgetting factor recursive least squares, Collaborative state estimation, double extended Kalman, multi-time scale

Collaborative state estimation of lithium-ion battery based on multi-time scale low-pass filter forgetting factor recursive least squares - double extended Kalman filtering algorithm

Tao Long[a], Shunli Wang[a*], Wen Cao[a], Pu Ren[a], Mingfang He[a], Carlos Fernandez[b]

[a]*School of Information Engineering, Southwest University of Science and Technology, Mianyang 621010, China;* [b]*School of Pharmacy and Life Sciences, Robert Gordon University, Aberdeen AB10-7GJ, UK.*

Abstract: For the lithium battery management system and real-time safety monitoring, two issues are of great significance, namely the ability to accurately update the model parameters in real time and to accurately estimate the state of charge and health. In this context, this thesis adopts the second-order RC equivalent circuit model and the forgetting factor recursive least squares - double extended Kalman filtering (FFRLS-DEKF) algorithm with multi-time scales and low-pass filter. forgetting factor recursive least squares is applied to conduct online parameter identification, and the traditional double extended Kalman filtering algorithm is optimized to evaluate the state of charge and model parameters in the micro-scale and macro-scale. In this way, the error caused by two different characteristics is reduced, and a low-pass filter is added to optimize the fluctuation problem of the estimated value of the model parameters. According to the experiment results, the maximum error between the model simulation value and the actual value of the terminal voltage is 0.0459 V. If the initial value of the state of charge deviates from the actual value, the maximum errors under BBDST and HPPC conditions record 0.0235 and 0.0048, respectively, the forgetting factor recursive least squares - double extended Kalman filtering algorithm with multi-time scales and low-pass filter is able to track the true value within 40 seconds. Furthermore, the lithium-ion battery state of health both reaches 98% under the two conditions. In summary, the experimental analysis shows that the algorithm helps reduce the influence of initial values on the results, thereby reducing error accumulation and improving the robustness.

Key words: Low pass filter; Second-order RC model; forgetting factor recursive least squares; Collaborative state estimation; double extended Kalman ; multi-time scale

***Corresponding author**: Shunli Wang. Tel: +86-15884655563. E-mail address: 497420789@qq.com.

1. Introduction

At present, new energy vehicles, aerospace, and many other emerging energy strategies are developing rapidly [1, 2]. Lithium-ion battery management systems (BMS) and real-time reliable detection systems have been regarded as the core technology of new energy systems [3, 4]. Lithium-ion batteries' number of cycles, cost, reliability, and safety problems are becoming increasingly prominent. The demand for technological breakthrough and theoretical innovation of high-quality lithium-ion battery is rapidly expanding [5]. The requirement of accurately updating the model parameters in real-time and accurately estimating the state of charge and health are increasing. There are many applications around us. For example, EV wireless charging and Wireless sensor Networks field[6, 7]. Electric Vehicle Charging Study[8]. The research and development of a new generation of high-end lithium-ion battery energy and intelligent real-time detection system is the key breakthrough of the national new energy research and development industry [9]. The in-depth research on lithium-ion batteries' state of charge and health by many industry personnel will be introduced in detail below [10].

In the initial estimation of the state of charge of the lithium-ion battery, the discharge experiment method is adopted to carry out a constant discharge of the lithium-ion battery and stop it when it reaches the cut-off voltage. This method is relatively simple and the obtained results are relatively accurate [11]. Still, it takes a long time and can not calculate the lithium-ion battery under the working state in real time. In order to make up for the deficiency of discharge experiment method, the ampere hour method is proposed to estimate state of charge [12]. Its principle is to calculate the total amount of charge and discharge charge in a period of time by giving state of charge value at a particular time. The estimated value can be obtained by superimposing the given value and calculated value [13]. There are some problems with ampere hour method, for example, its estimation error will accumulate over time and estimation accuracy depends on the initial value [14]. In order to solve the error accumulation problem of the ampere-hour method, Kalman Filter algorithm was proposed based on the ampere-hour [15]. This algorithm is mainly composed of prediction and update. It continuously iterates estimating state of charge, quickly tracks the real state of charge value and calculates the optimal estimate value [16]. However, Kalman Filter algorithm can only solve linear problems, and the estimation of state of charge is usually a nonlinear process, so it needs to linearize the nonlinear system [17]. When Kalman Filter can not solve the nonlinear problem, Extended Kalman Filter algorithm based on Kalman filter algorithm to solve the nonlinear system [18], by linearizing the nonlinear state space equation, Kalman filter algorithm to achieve state of charge estimation [19]. The authors propose a cubic Kalman filtering algorithm combining fuzzy adaptive and singular value decomposition in order to solve the problem of slow convergence time of cubic Kalman algorithm[20].

Four kind of algorithms based on Kalman filter extension are introduced in detail (extended Kalman filter, unscented Kalman filter, cubature Kalman filter and ensemble Kalman filter), the advantages and disadvantages, estimation accuracy and anti-interference ability of these four algorithms were compared in detail [21]. The author proposed a novel Adaptive Square root Extended Kalman filter based on extended Kalman filter algorithm, which solved the filtering divergence problem and ensured non-negative deterministic in [22]. In addition to the author proposed a correntropy - weighted least squares - extended Kalman filter algorithm to estimate state of charge, and the error can be effectively reduced under the condition of non-Gaussian noise in [23]. Aiming at the problem of battery parameter marginalization and ageing, the authors estimate state of charge accurately by volume Kalman filter combined with recursive least squares in [24]. The author focuses on the fractal-order adaptive extended Kalman filter, which can quickly track the unknown variance in [25]. An estimation method with an adaptive feedback compensator is proposed, which can improve state of charge estimation performance and fast convergence in [26].

With the rapid development of society, the use frequency of lithium-ion battery products is increasing [27], and the aging problem of lithium-ion battery is becoming increasingly apparent. In order to know the aging degree of battery in real time and accurately [28], we introduce the battery State of Health (SOH). The battery health status is defined as the ratio of the capacity released by the power battery from the full charge state to the cut-off voltage at a certain rate to the standard capacity under standard conditions [29]. This ratio is a manifestation of the battery health status and conforms to most current lithium-ion batteries [30]. At present, there are several methods to estimate the health status of lithium-ion batteries: neural network algorithm. The abandon the traditional equivalent circuit method and independent of model, a method of state of health estimation based on incremental capacity and fusion of wavelet neural network and genetic algorithm is proposed in [31]. The authors developed a neural network that used more than 110,000 measurements to train and validate the model in [32]. The author proposes a new multi-scale state of health model to solve the capacity degradation problem, and finally constructs a prediction framework based on wavelet neural network and integrated learning network in [33]. Model estimation method, a model-based voltage construction method is proposed to eliminate unfavorable numerical conditions and reshape incremental capacity (IC) curves in [34]. The author proposes a novel state of health estimator based on fusion, which has a high estimate of intensive reading in [35]. The author proposed a battery health assessment framework based on fuzzy comprehensive evaluation (FCE) and improved multiple grey model (IMGM) to optimize multiple health indicators (MHIs) system to reduce the influence of Health indicator (HI) error on the overall prediction results in [36]. Data driven and Support vector machine [37-39]. The author proposes an improved sine-cosine algorithm based on the two-order RC model [40]. The author takes machine learning as the starting point, analyzes and compares five popular intelligent algorithms, and provides some enlightenment for maximum likelihood method to estimate state of health [41].

With the increasing accuracy requirements of the algorithm, this paper proposes a multi-time scale low-pass filter forgetting factor recursive least squares method - double extended Kalman filter (FFRLS-DEKF) co-estimation algorithm for state of charge and state of health. Based on extended Kalman filter algorithm, a double extended Kalman filter is used. One Kalman filter is used to estimate the slow time-varying characteristics of parameters and the other Kalman filter is used to estimate the fast time-varying characteristics of system states, which can effectively solve the problem of different time scales of system parameters and system states. In the parameter estimation, a low pass filter is introduced to optimize the parameter estimation result, which improves the accuracy of state of health estimation value. The advantage of the whole algorithm in terms of computational efforts is that it calculates two kinds of variables at different time scales, which meets the different requirements of system parameters and system states and improves the accuracy of estimation. However, the disadvantage is that it requires a large amount of calculation and has certain requirements for equipment performance.

2. Mathematical analysis

2.1 2-RC equivalent modeling

The equivalent circuit model is inseparable from the charge-discharge experiment, and the performance parameters of lithium-ion battery are studied by Hybrid Pulse Power Characterization Test (HPPC) [42]. In order to accurately estimate state of charge, state of health and other model parameters under lithium-ion battery operation, the second-order RC equivalent circuit model is selected in this paper [43]. Compared with the Thevenin equivalent circuit model [44], the second-order RC circuit model has an additional RC loop representing dynamic response, as shown in Fig. 1.

[Insert Figure 1]

Fig. 1 Second order RC equivalent circuit model

In this model, U_b represents the voltage source of the lithium-ion battery, which varies with state of charge, Ri represents the ohmic internal resistance of the battery [45], R_1 and R_2 both represent the polarization resistance of the battery, U represents the measured terminal voltage, and in the equivalent circuit, RC circuit composed of R_1 and C_1 represents the process of rapid voltage change in the electrochemical reaction inside the battery [46]. The RC circuit composed of R_2 and C_2 represents the process in which the voltage of the electrochemical reaction inside the battery changes slowly, and I is the direction of the current circuit [47]. According to Kirchhoff's voltage law, the KVL equation of the circuit can be obtained as shown in Equation (1).

$$\begin{cases} U_b = U + U_i + U_1 + U_2 \\ \dfrac{dU_1}{d_t} = -\dfrac{U_1}{R_1C_1} + \dfrac{I}{C_1} \\ \dfrac{dU_2}{d_t} = -\dfrac{U_2}{R_2C_2} + \dfrac{I}{C_2} \end{cases} \tag{1}$$

In order to estimate the charged state, it is necessary to establish the system's state equation, observation equation and parameter estimation parameter equation, and equation (2) can be obtained by discretization Equation (1).

$$\begin{cases} x_{k,l+1} = f(x_{k,l},\theta_k,u_{k,l}) + w_{k,l} \\ Y_{k,l} = g(x_{k,l},\theta_k,u_{k,l}) + v_{k,l} \\ \theta_{k+1} = \theta_k + \rho_k \end{cases} \tag{2}$$

According to the second order RC equivalent circuit model, $[SOC\ U_1\ U_2]$ was selected as the state variable, and combined with equation (2) and state of charge definition discretization, the equation (3) was obtained as follows.

$$\begin{cases} \begin{bmatrix} SOC_{k+1} \\ U_{1,k+1} \\ U_{2,k+1} \end{bmatrix} = \begin{bmatrix} 1 & 0 & 0 \\ 0 & 1-{T}/{\tau_1} & 0 \\ 0 & 0 & 1-{T}/{\tau_2} \end{bmatrix} \# \# \\ U_{b,k+1} = U(SOC,k+1) + U_i + U_1 + U_2 \end{cases} \tag{3}$$

In equation (3), T is sampling time, τ_1 and τ_2 equal to R_1C_1 and R_2C_2 respectively, the relation of $SOC - OCV$ can be obtained by polynomial fitting. Forgetting Factor Recursive Least Square method is used for polynomial fitting of data, the variation of parameters is not obvious, the order of polynomial is increasing, the more likely produce oscillations. In polynomial fitting of experimental data, it is found that the effect of polynomial fitting with sixth order is equivalent to that of polynomial fitting with seventh order due to the existence of oscillation phenomenon. Therefore, sixth-order polynomial is chosen as the fitting target. $U(SOC,k+1)$ can be expressed as shown in Equation (4).

$$U(SOC,k+1) = K_0 + K_1SOC + K_2SOC^2 + K_3SOC^3 + K_4SOC^4 + K_5SOC^5 + K_6SOC^6 \tag{4}$$

Where k and l represent the macroscopic system parameters and the microscopic system state indicators respectively, where $x_{k.l}$ is the state equation of the system, $U_{k,l}$ is the input matrix, $Y_{k,l}$ is the observation equation at this moment, where $w_{k,l}$ and ρ_k are the process noise of the observation equation and parameter equation, $v_{k,l}$ is the observation noise. Both system noise and observation noise are gaussian white noise, and their variances are expressed as Q and R. Where K is an undetermined coefficient, which can be obtained by fitting open circuit voltage (OCV) and state of charge.

2.2 FFRLS Parameter identification

Choosing 4.2V/70Ah term-power lithium-ion battery, which has the advantages of high energy density[48], good cycle performance and long battery life. In the lithium-ion battery management system (BMS), the Hybrid Pulse Power Characterization Test (HPPC) is carried out with ternary lithium-ion battery as the experimental object [49]. The principle is to discharge the battery every SOC=0.1 to get the variation rule of each parameter [50]. The voltage transformation curve is shown in Figure 2 (a), and the current curve is shown in Figure 2(b).

[Insert Figure 2 (a)] [Insert Figure 2 (b)]

(a) HPPC voltage curve (b) HPPC current curve

Fig. 2 Voltage and current curve under HPPC test

The variation curves of various parameters are obtained by Hybrid Pulse Power Characterization experiment and the parameters of the second-order RC model are identified by using the Forgetting Factor Recursive Least Square (FFRLS) [51]. In the identification process, the function of the forcing factor is to give a small weight to the data with a long running time, while the latest observation data occupy a large weight. The identification process is as follows:

The second-order RC equivalent circuit model is transformed into the mathematical form of the least square method, as shown in Equation (5).

$$U_b = \left(\frac{R_1}{R_1C_1s+1} + \frac{R_2}{R_2C_2s+1} + R_i\right)\mathrm{I} + U \tag{5}$$

As in equation (5), let $\tau_1 = R_1C_1$ and $\tau_2 = R_2C_2$, Substitute it into Equation (5) to obtain:

$$\begin{aligned}\tau_1\tau_2U_bs^2 + (\tau_1+\tau_2)U_bs + U_b = s^2\tau_1\tau_2R_iI + s[R_1\tau_2 + R_2\tau_1 + R_i(\tau_1+\tau_2)]I \\ + (R_1+R_2+R_i)I + s^2\tau_1\tau_2U + s(\tau_1+\tau_2)U + U\end{aligned} \tag{6}$$

As in equation (6), let $a=\tau_1\tau_2$, $b=\tau_1+\tau_2$, $c=R_1+R_i+R_2$, $d=R_1\tau_2+R_2\tau_1+R_i(\tau_1+\tau_2)$, Then the above equation can be simplified to equation (7).

$$aU_b s^2+bU_b s+U_b=as^2R_iI+d\,sI+cI+as^2U+b\,sU+U \tag{7}$$

Substitute $s=\frac{[x(k)-x(k-1)]}{T}$, $s^2=[x(k)-2x(k-1)+x(k-2)]/T$into equation (7) for discretization, where T is the sampling time, as shown below:

$$U_b(k)-U(k)=\frac{-bT-2a}{T^2+bT+a}[U(k-1)-U_b(k-1)]+\frac{a}{T^2+bT+a}[U(k-2)-U_b(k-2)]+ \\ \frac{cT^2+dT+aR_i}{T^2+bT+a}I(k)+\frac{-dT-2aR_i}{T^2+bT+a}I(k-1)+\frac{aR_i}{T^2+bT+a}I(k-2) \tag{8}$$

Simplify (8), we can get Eq.(9) as follow.

$$U_b(k)-U(k)=k_1[U(k-1)-U_b(k-1)]+k_2[U(k-2)-U_b(k-2)]+ \\ k_3I(k)+k_4I(k-1)+k_5I(k-2) \tag{9}$$

Each coefficient in equation (9) can be expressed as follows:

$$\begin{cases} k_1=\dfrac{-bT-2a}{T^2+bT+a} \\ k_2=\dfrac{a}{T^2+bT+a} \\ k_3=\dfrac{cT^2+dT+aR_i}{T^2+bT+a} \\ k_4=\dfrac{-dT-2aR_i}{T^2+bT+a} \\ k_5=\dfrac{aR_i}{T^2+bT+a} \end{cases} \tag{10}$$

As in equation (10), let θ=$[k_1,k_2,k_3,k_4,k_5]^T$, bring it into the forgetting factor recursive least squares algorithm, and solve the parameter values of the second-order RC equivalent circuit from the identification results. The forgetting factor recursive least squares recurrence equation is as follows:

$$\begin{cases} \hat{\theta}(k+1)=\hat{\theta}(k)+K(k+1)[y(k+1)-\phi^T(k+1)\hat{\theta}(k)] \\ K(k+1)=P(k+1)\phi(k+1)[\phi^T(k+1)P(k)\phi(k+1)+\lambda]^{-1} \\ P(k+1)=\lambda^{-1}[I-K(k+1)\phi^T(k+1)]P(k) \end{cases} \tag{11}$$

Where *P(k)* is the covariance matrix, *ϕ(k)* = $[v_{k-1}\, v_{k-1}\, I_k\, I_{k-1}\, I_{k-2}]$, *K* is the gain, *λ* It is a genetic factor, generally 0< *λ*< 1, when the λ gets smaller value, the better the tracking effect of the algorithm, but it will cause the fluctuation of the algorithm λ, When l is taken, it is the standard least squares recursive method. Through continuous iterative calculation, the results of each time can be obtained θ. The value of R_i, R_1, R_2, C_1 and C_2 are calculated from equation (12).

$$\begin{cases} R_{\mathrm{i}} = \dfrac{k_3 - k_4 + k_5}{1 + k_1 - k_2} \\ \tau_1\tau_2 = \dfrac{T^2(1 + k_1 - k_2)}{4(1 - k_1 - k_2)} \\ \tau_1 + \tau_2 = \dfrac{T(1 + k_2)}{1 - k_1 - k_2} \\ R_{\mathrm{i}}\tau_1 + R_{\mathrm{i}}\tau_2 + R_1\tau_2 + R_2\tau_1 = \dfrac{T(k_3 - k_5)}{1 - k_1 - k_2} \\ R_{\mathrm{i}} + R_1 + R_2 = \dfrac{k_3 + k_4 + k_5}{1 - k_1 - k_2} \end{cases} \tag{12}$$

2.3 Multi time scale double extended Kalman filter algorithm

The traditional dual extended Kalman filter (DEKF) is used to estimate the battery system parameters and system state at the same time [52]. In each iterative calculation, the state filter of extended Kalman filter uses parameter estimation $\hat{\theta}_{\mathrm{k}}^{-}$ The parameter filter of extended Kalman filter uses the current state estimation value x_{k} estimate the system model parameters. Since the traditional double extended Kalman filter can only estimate parameters and states at the same time, a multi time scale double extended Kalman filter is proposed in this paper. From equation (2), it can predict the state value of the system at the micro scale, predict the parameter value of the model at the macro scale, and provide stable system parameters and state estimation. The recursive process of dual extended Kalman filter is as follows:

Step 1: initialize system status value and parameter value

$$\hat{\theta}_0 = \mathrm{E}[\theta],\ P_{\theta_0} = \mathrm{E}[(\theta_0 - \hat{\theta}_0)(\theta_0 - \hat{\theta}_0)^T],\ \hat{x}_0 = E[x],\ P_{x0} = \mathrm{E}[(x_0 - \hat{x}_0)(x_0 - \hat{x}_0)^T] \tag{13}$$

Step 2: parameter filter time update equation

$$\hat{\theta}_l^{\,-} = \hat{\theta}_{l-1}, P_1^{-} = P_1 + Q^{\theta} \tag{14}$$

Step 3: parameter filter measurement update equation

$$\begin{cases} \mathrm{K}_1 = P_l C_l^T [C_l P_l C_l^T + \mathrm{R}_1]^- \\ \hat{\theta}_1 = \hat{\theta}_1^- + \mathrm{K}_1 Y_l - \mathrm{K}_1 g(x_k, \hat{\theta}_l^-, u_k) \\ P_{\theta_l} = (I - \mathrm{K}_1 C_l) P_1^- \end{cases} \tag{15}$$

Step 4: state filter time update equation

$$\hat{x}_k^- = f(\hat{x}_{k-1}, \hat{\theta}_{k-1}, u_k), P_k^- = A \hat{P}_{k-1} A^T + Q_{k-1} \tag{16}$$

Step 5: state filter measurement update equation

$$\begin{gathered} \mathrm{K}_k = P_k C_k^T [C_k P_k^- C_k^T + \mathrm{R}_k]^- \\ \hat{x}_k = \hat{x}_k^- + \mathrm{K}_k Y_k - \mathrm{K}_k g(x_k, \hat{\theta}_l^-, u_k) \\ P_k = (I - \mathrm{K}_k C_k) P_k^- \end{gathered} \tag{17}$$

The calculation method of A, C_k and C_l is as follows

$$\mathrm{A} \triangleq \frac{\partial f(x_{k,l}, \theta_k, u_{k,l})}{\partial \mathrm{x}},\ C_k \triangleq \frac{\partial g(x_{k,l}, \theta_k, u_{k,l})}{\partial x},\ C_l \triangleq \frac{\partial g(x_{k,l}, \theta_k, u_{k,l})}{\partial \theta} \tag{18}$$

Where: $\hat{\theta}_0$ is the initial value of the parameter value, which can be calculated according to the model, P_{θ_0} is the parameter value of the parameter error covariance matrix, $\hat{\mathrm{x}}_0$ is the initial value of state quantity, $\mathrm{P}_{\mathrm{x}_0}$ the initial value of the state error covariance matrix, all of which are the initial values in the algorithm, $\hat{\theta}_1$ is the estimated value of the minimum variance of the parameter at time *l*, $\hat{\mathrm{x}}_\mathrm{k}$ is the minimum variance estimate of the parameter at time *k*, K_k and K_1 is Kalman gain, C_k is the state transition matrix at time *k*. it should be noted that C_k in parameter filtering refers to the total derivative of the measurement equation with respect to the parameters. We need to decompose the total derivative into partial derivatives and the process is as follows:

$$C_l \triangleq \frac{\partial g(x_{k,l}, \theta_k, u_{k,l})}{\partial \theta} = \frac{\partial g(x_{k,l}, \hat{\theta}_l^-, u_{k,l})}{\partial \hat{\theta}_l^-} + \frac{\partial g(x_{k,l}, \hat{\theta}_l^-{}_l, u_{k,l})}{\partial \hat{x}_\mathrm{k}} \times \frac{\mathrm{d}\hat{x}_k}{d\hat{\theta}_l^-} \tag{19}$$

$$\frac{\mathrm{d}\hat{x}_k}{d\hat{\theta}_l^-} = \frac{df(x_{k-1,l}, \hat{\theta}_l^-, u_{k-1,l})}{d\hat{\theta}_l^-} = \left(\frac{\partial f(x_{k-1,l}, \hat{\theta}_l^-, u_{k-1,l})}{\partial \hat{\theta}_k^-} + \frac{\partial f(x_{k-1,l}, \hat{\theta}_l^-, u_{k-1,l})}{\partial \hat{x}_{k-1}} \times \frac{d\hat{x}_{k-1}}{d\hat{\theta}_l^-} \right) \tag{20}$$

$$\frac{d\hat{x}_{k-1}}{d\hat{\theta}_l^-} = \frac{d\hat{x}_{k-1}^-}{d\hat{\theta}_l^-} - \mathrm{k}_{k-1}^x \frac{dg(x_{k-1,l}, \hat{\theta}_l^-, u_{k-1,l})}{d\hat{\theta}_l^-} \tag{21}$$

The flowchart of the multi time scale double extended Kalman filter algorithm is shown in Fig.3 and the specific steps are as follows.

[Insert Figure 3]

Fig.3 The flowchart of the multi time scale double extended Kalman filter

Step 1 : Initialize the multi time scale dual extended Kalman filter algorithm and select the appropriate values of $\hat{\theta}_0$, P_{θ_0}, $\hat{x}_0$ and P_{x_0} using Eq.(13).

Step 2: Under macro scale, according to the slow time characteristic of the parameter, the parameter filter starts to update, $\hat{\theta}_l^{\,-}$ and P_l^- are calculated from Eq.(14).

Step 3: The obtained parameter value $\hat{\theta}_l^{\,-}$ and P_l^- is brought into Eq. (15) for parameter filter measurement update to complete a parameter filtering process. After l return to the second step to continue the parameter iterative calculation.

Step 4: Under micro scale, From the obtained $\hat{\theta}_k^{\,-}$, $\hat{x}_0$ and P_{x0}, calculate $\hat{x}_k^{\,-}$ and P_k^- according to Eq.(16).

Step 5: Based on the obtained status update value $\hat{x}_k^{\,-}$ and P_k^-, calculate the status measurement update value by Eq.(17). After k return to step four to start a new round of system status update.

The whole process of multi-time scale dual extended Kalman filter algorithm can be realized through the five-step iterative calculation process.

2.4 Low pass filtering combined iterative calculation

The loss of lithium-ion will lead to the attenuation of lithium-ion battery capacity and the further aging of lithium-ion battery state. In order to capture this attenuation, the state of health (SOH) is introduced, SOH of lithium-ion battery represents the capacity of the current battery to store electric energy relative to the new battery, and usually represents the state of the battery from the beginning to the end of its life in the form of percentage, which is used to quantitatively describe the performance state of the current battery. When the battery is produced, the state of health is 100%, which means 1. In this part, which is defined as the ratio of the actual maximum available capacity Q_{max} to the rated capacity Q_N. In this paper, the multi-time scale dual extended Kalman filter algorithm is used to continuously estimate the battery capacity parameters in real time in view of the time-varying characteristics of lithium-ion battery parameters at the macro scale, so as to reduce the estimation error of SOH. The calculation equation of SOH is shown in Eq.(22).

$$\mathrm{SOH} = \frac{Q_{max}}{Q_N} \times 100\% \tag{22}$$

During the estimation of the parameter filter, the estimated capacity occasionally fluctuates greatly. In order to obtain the accurate state of health estimation value, a low-pass filter is added to the parameter estimation part of the algorithm. The low-pass filtering method uses the sampling value and the output value of the last filtering to get the effective filtering value, so that the output has a feedback effect on the input, reducing the amplitude of the result fluctuation, and its frequency value will not change, nor will it change its real value. As shown in Eq. (23).

$$Y(n) = \alpha X(n) + (1-\alpha)Y(n-1) \tag{23}$$

In Eq.(23), $Y(n)$ is the filter output value, $Y(n-1)$ is Last filter output value, $X(n)$ is sample value, α is Filter coefficients.

In order to better demonstrate the running process of the multi-time scale low-pass filter forgetting factor recursive least squares - double extended Kalman filtering algorithm, the flow chart of the multi-time scale low-pass filter forgetting factor recursive least squares - double extended Kalman filtering algorithm is shown in Fig.4.

[Insert Figure 4]

Fig.4 Flow chart of the multi-time scale low-pass filter FFRLS - DEKF algorithm

The algorithm starts with initialization of the program. In the first step the data obtained through experiments are imported into the forgetting factor recursive least squares algorithm for online parameter identification. In the second step, the obtained data for each parameter are applied to the multi-time scale double extended Kalman filtering algorithm for continuous iterative computation. Final output state of charge estimate, before outputting state of health, low-pass filtering optimizes the output for the estimated value.

3. Experimental analysis

3.1 System platform design

In this study, a ternary lithium-ion battery with a standard capacity of 70Ah was used as the research object. To verify the accuracy of the proposed algorithm, a small-scale test platform was built through the existing conditions in the laboratory. Fig.5 depicts the structure of the experimental platform and Tab.1 describes the specifications of the BMS and lithium-ion battery.

[Insert Figure 5]

Fig.5 Experimental lithium-ion battery test platform

As shown in Fig.5, the structure of test platform includes: (a) Programable constant temperature test box, it is used to control the ambient temperature and prevent changes in ambient temperature from affecting the results of the experiment. (b) Ternary lithium-ion battery. (c) High-rate power battery charge-discharge tester (CT-4016-5 V100A-NTFA), it is used for charge and discharge experiments. (d) BMS performance control systems. (e) PC serves as the control hub.

Tab.1 Lithium-ion battery and BMS specifications

[Insert Table 1]

3.2 FFRLS algorithm verification

Through the above theoretical analysis, the experimental data obtained from HPPC test was brought into the forgetting factor recursive least square method (FFRLS) to obtain the real-time data of each parameter. Each result was plotted by Origin, and the estimated voltage value was compared with the real voltage value to verify the accuracy of the algorithm.

[Insert Figure 6 (a)]

(a) R_i identification result curve

[Insert Figure 6 (b)]

(b) R_1 identification result curve

[Insert Figure 6 (c)] [Insert Figure 6 (d)]

(c) R_2 identification result curve (d) C_1 identification result curve

Fig. 6 Estimated values of FFRLS parameters under Second RC model

Fig.6 shows the four parameter results of forgetting factor recursive least squares algorithm edge identification, (a) - (c) are the identification results of ohmic internal resistance and two polarization resistances of the battery respectively, (d) is the identification result of polarization capacitance. At the initial stage of battery discharge, the parameters fluctuate greatly. With the continuous decrease of SOC, the parameters gradually tend to be stable under the estimation of forgetting factor recursive least squares algorithm.

[Insert Figure 7 (a)] [Insert Figure 7 (b)]

(a) Comparison between simulated voltage and the actual voltage (b) FFRLS simulation voltage error result curve

Fig. 7 Second order RC model voltage validation and error curve

Fig. 7 (a) shows the comparison between the simulated voltage and the actual voltage obtained by the forgetting factor recursive least squares algorithm. It can be seen from the figure that the results obtained by the forgetting factor recursive least squares algorithm are basically consistent with the real results. At the end, the error is largely due to the large voltage fluctuation of the lithium-ion battery. It can be seen from (b) that the maximum voltage error of forgetting factor recursive least squares algorithm in verifying the model is 0.0459V, and the error is within the allowable range. Through the result analysis, forgetting factor recursive least squares has good accuracy in the process of parameter identification.

3.2 HPPC condition verification

Through the above theoretical analysis, this section will verify whether the multi time scale forgetting factor recursive least squares - double extended Kalman filtering algorithm based on low-pass filter is accurate when the initial SOC value is equal to 0.6, the fast time scale l is equal to 1s and the slow time scale k is equal to 80s under (Hybrid Pulse Power Characteristic) HPPC working conditions, and whether the capacity value estimated by parameter filter is stable and reliable through low-pass filter. In order to intuitively see the accuracy of the algorithm, extended Kalman filter (EKF) and double extended Kalman filter (DEKF) will be verified under the same conditions to compare whether the three algorithms are better than the other two algorithms at 25 degrees ambient temperature.

[Insert Figure 8 (a)]

(a) Estimated SOC and true SOC curve under HPPC condition

[Insert Figure 8 (b)]

(b) SOC error curve under HPPC condition

[Insert Figure 8 (c)]

(c) Estimated capacity and low-pass filter capacity under HPPC condition

[Insert Figure 8 (d)]

(d) SOH curve under HPPC working condition

Fig. 8 Three different algorithms SOC estimation, low pass filtering and SOH results under HPPC

When the initial value is equal to 0.6, by verifying the extended Kalman filter (ekf), double extended Kalman filter (dekf), and comparing the multi time scale forgetting factor recursive least squares - double extended Kalman filtering algorithm based on the low-pass filter (The algorithm is represented in the legend as r-dekf) with the real SOC, it can be seen from Fig. 8 (b) that the maximum error of forgetting factor recursive least squares - double extended Kalman filtering algorithm is 0.0048, the maximum error of double extended Kalman filtering algorithm is 0.0225, and the maximum error of extended Kalman filtering algorithm is 0.0867 under Hybrid Pulse Power Characteristic working condition. In addition, forgetting factor recursive least squares - double extended Kalman filtering algorithm can quickly converge to the accurate value in 40 seconds. On the contrary, the convergence speed of the other two algorithms is slower than that forgetting factor recursive least squares - double extended Kalman filtering algorithm. In Fig.8 (c) f – C denotes the curve after estimation by low-pass filtering. It can be seen from Fig.8 (c) that the capacity estimated by forgetting factor recursive least squares - double extended Kalman filtering algorithm fluctuates greatly, but after the low-pass filtering algorithm, the capacity estimation tends to be stable, and the battery state of health (SOH) is determined by the estimated filter value Fig.8 (d) shows that the state of health lithium-ion battery is at 98%. In order to further verify the multi time scale reliability of the algorithm, it will be verified when the slow time scale *k* becomes 20s.

[Insert Figure 9 (a)] [Insert Figure 9 (b)]

(a) Estimated SOC and true SOC curve under HPPC condition (b) SOC error curve under HPPC condition

Fig. 9 Comparison diagram of real SOC and estimated SOC, estimation error diagram.

It can be seen from Fig. 9 (a) and (b) that the convergence of the algorithm is worse than that when the slow time scale is 80s. Before SOC = 0.4, the algorithm error under Hybrid Pulse Power Characteristic working condition has reached 0.0068, the maximum error when the full scale is 80s is 0.0048, and the error continues to accumulate. The analysis shows that when the time *k* of the slow time scale is small, the algorithm will also produce large errors. Therefore, it shows that a reasonable time is particularly important when selecting the slow time scale.

To further verify the stability and accuracy of the multi-time scale low-pass filter forgetting factor recursive least squares - double extended Kalman filtering algorithm under different temperature environments, the battery was placed in an environment of 35 degrees celsius for the same Hybrid Pulse Power Characteristic experiments. The obtained results are shown below.

[Insert Figure 10 (a)] [Insert Figure 10 (b)]

(a) Estimated SOC and true SOC curve under HPPC (b) SOC error curve under HPPC condition

condition

[Insert Figure 10 (c)] [Insert Figure 10 (d)]

(c) SOH curve under HPPC working condition (d) Low-pass filtering effect

Fig.10 SOC and SOH curves output by the algorithm at 35 degrees ambient temperature

The data obtained from the Hybrid Pulse Power Characteristic test at an ambient temperature of 35 degrees and the results obtained after the algorithm can be seen that the multi time scale low-pass filter forgetting factor recursive least squares - double extended Kalman filtering algorithm has a maximum error of 0.0172 in estimating the SOC, which is within the allowable error range. the difference between the SOH output curve in the SOH output curve and the SOH curve in Figure 8 is within 0.01. The stability of the algorithm under different temperature environments is demonstrated. Since zero SOC is a nonexistent quantity in reality, the experimental SOC less than 0.2 is used here only as a reference.

3.3 BBDST condition verification

In order to verify the accuracy of multi time scale forgetting factor recursive least squares - double extended Kalman filtering algorithm based on low-pass filter under different working conditions, this section verifies the algorithm under Beijing bus dynamic stress test (BBDST) at 25 degrees ambient temperature. When the initial SOC value is equal to 0.6, the slow time scale k is equal to 80s, and the fast time scale l is equal to 1s, calculate the system state value, estimate the capacity value through the parameter filter, and optimize through the low-pass filter, then estimate the SOH value. The results are shown in the figure below.

[Insert Figure 11 (a)] [Insert Figure 11 (b)]

(a) Estimated SOC and true SOC curve (b) SOC error curve

[Insert Figure 11 (c)] [Insert Figure 11 (d)]

(c) Estimated capacity and low-pass filter capacity diagram (d) SOH curve

Fig. 11 Three different algorithms SOC estimation, low pass filtering and SOH results under BBDST

It can be seen from Fig.11 that under Beijing bus dynamic stress test working condition, the multi time scale forgetting factor recursive least squares - double extended Kalman filtering algorithm based on low-pass filter (The algorithm is represented in the legend as r-dekf) is the closest to the real value, and its maximum error is 0.0235, the maximum error of double extended Kalman filtering algorithm is 0.0335, and the maximum error of extended Kalman filtering algorithm is 0.0762. It can be seen that forgetting factor recursive least squares - double extended Kalman filtering algorithm has the best effect in estimating state of charge. As can be seen from Fig.11 (c), the estimation of the algorithm fluctuates greatly before the low-pass filter algorithm is added, and the estimation capacity is more gentle and less fluctuated after the low-pass filter algorithm is added. Its health state is about 98%, which is consistent with the estimated state of health under Hybrid Pulse Power Characteristic working conditions. It also shows the new reliability of the algorithm in jointly estimating state of charge and state of health under two working conditions. At the same time, the change of state of charge estimation value when state of charge slow time scale k = 20s is also verified under Beijing bus dynamic stress test working conditions.

[Insert Figure 12 (a)] [Insert Figure 12 (b)]

(a) Estimated SOC and true SOC curve (b) SOC error curve

Fig. 12 Result of FFRLS-DEKF method deviating from the correct initial SOC. Result of battery health status

As can be seen from Fig. 12, when the slow time scale is 20 seconds, the algorithm will accumulate and increase the error when SOC = 0.6, and the error has reached 0.03 when SOC = 0.2. Therefore, through the analysis of two working conditions, the multi time scale forgetting factor recursive least squares - double extended Kalman filtering algorithm based on low-pass filter can reflect a good state of charge estimation accuracy.

Similarly to verify the accuracy and stability of the multi-time scale low-pass filter forgetting factor recursive least squares - double extended Kalman filtering algorithm estimation under Beijing bus dynamic stress test

(BBDST)working condition. Two ambient temperature experiments were conducted on the battery again, one at 35 degrees ambient temperature and the other at 15 degrees ambient temperature. The algorithm will estimate the SOC and SOH under the obtained experimental data, the estimated results are as follows.

[Insert Figure 13 (a)] [Insert Figure 13 (b)]

(a) Estimated SOC and true SOC curve (b) SOC error curve

[Insert Figure 13 (c)] [Insert Figure 13 (d)]

(c) SOH estimation curve (d) Estimated capacity and low-pass filter capacity diagram

Fig.13 Algorithm SOC and SOH results for different ambient temperature BBDST conditions

In Figure 13, r-dekf-15, SOH-15 and f-C-15 denotes the estimated curve of the algorithm at 15 degrees. r-dekf-35, SOH-35 and f-C-15 denotes the estimated curve of the algorithm at 35 degrees. The algorithm has a maximum error of 0.0355 at an ambient temperature of 15 deg. with a maximum error of 0.0115 at an ambient temperature of 35 deg. In the SOH estimation, both ambient temperature estimates result in values with an error no greater than 0.02 compared to the error at 25 deg. The results show that the algorithm is able to have good stability at different ambient temperatures. Since zero SOC is a nonexistent quantity in reality, the experimental SOC less than 0.2 is used here only as a reference.

4. Conclusions

Considering the continuous improvement of the requirements for real-time condition monitoring and reliability of lithium-ion batteries. In this paper, HPPC and BBDST experimental data are obtained through experiments. An innovative multi-time scale low-pass filter forgetting factor recursive least squares - double extended Kalman filtering algorithm is proposed to solve the multi-time scale and parameter identification problem, which cannot be solved by traditional double extended Kalman filtering and extended Kalman filtering algorithm. forgetting factor recursive least squares algorithm is used to online identify the parameters of the second-order RC equivalent circuit model, which effectively solves the problem of real-time parameter updating, it is verified by MATLAB simulation. The multi-time scale double extended Kalman filtering algorithm performs state estimation and parameter estimation at macro and micro scales respectively, it effectively solves the multi-time scale problem. The low pass filter solves the problem of capacitance fluctuation in parameter estimation and is used as a representation of the state of health. Experimental results show that the low-pass filter multi-time scale forgetting factor recursive least squares - double extended Kalman filtering algorithm has good performance in joint estimation of SOC and SOH.

Acknowledgments

The work was supported by National Natural Science Foundation of China (No. 62173281, 61801407).

DATA AVAILABILITY STATEMENT

Data available on request from the authors	The data that support the findings of this study are available from the corresponding author upon reasonable request.

References

1. Chen, Y., A. Dou, and Y. Zhang, *A Review of Recycling Status of Decommissioned Lithium Batteries.* Frontiers in Materials, 2021. **8**: p. 1-12.
2. Hsieh, Y.-C., L.-R. Yu, and M.-F. Yang, *A charge equalization scheme for battery string with charging current allocation.* International Journal of Circuit Theory and Applications, 2021. **49**(9): p. 2935-2945.
3. Kulova, T.L., et al., *A Brief Review of Post-Lithium-Ion Batteries.* International Journal of Electrochemical Science, 2020. **15**(8): p. 7242-7259.
4. Pourjafar, S., et al., *A bidirectional multiport DC-DC converter applied for energy storage system with hybrid energy sources.* International Journal of Circuit Theory and Applications, 2021. **49**(8): p. 2453-2478.
5. Du, G., et al., *Overview of research on thermal safety of lithium-ion batteries.* Energy Storage Science and Technology, 2019. **8**(3): p. 500-505.
6. Locorotondo, E., et al., *Design of a Wireless Charging System for Online Battery Spectroscopy.* Energies, 2021. **14**(1).
7. Lajara, R., J.J. Perez-Solano, and J. Pelegri-Sebastia, *Predicting the Batteries' State of Health in Wireless Sensor Networks Applications.* Ieee Transactions on Industrial Electronics, 2018. **65**(11): p. 8936-8945.
8. Zhao, Q., et al., *A study on combined multi-resonance converter for on-board charging of electric vehicles.* International Journal of Circuit Theory and Applications, 2021.
9. Liu, Y.-z., et al., *Recent advances in graphene materials used in Li-S batteries.* New Carbon Materials, 2020. **35**(1): p. 1-11.

10. Liang, H., et al., *A review of current research on the formation mechanism of lithium batteries.* Energy Storage Science and Technology, 2021. **10**(2): p. 647-657.

11. Lu, J., et al., *Mathematical Modeling and Frequency-Domain Characteristics of a Periodic Pulse-Discharged Lithium-Ion Battery System.* Ieee Transactions on Industry Applications, 2021. **57**(2): p. 1801-1809.

12. Liu, Z., et al., *Accurate and Efficient Estimation of Lithium-Ion Battery State of Charge with Alternate Adaptive Extended Kalman Filter and Ampere-Hour Counting Methods.* Energies, 2019. **12**(4): p. 1024-1054.

13. Xiong, X., et al., *A novel practical state of charge estimation method: an adaptive improved ampere-hour method based on composite correction factor.* International Journal of Energy Research, 2020. **44**(14): p. 11385-11404.

14. Zhang, L., et al., *High-safety separators for lithium-ion batteries and sodium-ion batteries: advances and perspective.* Energy Storage Materials, 2021. **41**: p. 522-545.

15. Reddy, M.V., et al., *Brief History of Early Lithium-Battery Development.* Materials, 2020. **13**(8): p. 2-26.

16. Liu, H., et al., *Comparisons on Kalman-Filter-Based Dynamic State Estimation Algorithms of Power Systems.* Ieee Access, 2020. **8**: p. 51035-51043.

17. Mahboub, V., et al., *On robust constrained Kalman filter for dynamic errors-in-variables model.* Survey Review, 2020. **52**(372): p. 253-260.

18. Garcia, R.V., et al., *Nonlinear filtering for sequential spacecraft attitude estimation with real data: Cubature Kalman Filter, Unscented Kalman Filter and Extended Kalman Filter.* Advances in Space Research, 2019. **63**(2): p. 1038-1050.

19. Zhengxin, J., et al., *An Immune Genetic Extended Kalman Particle Filter approach on state of charge estimation for lithium-ion battery.* Energy, 2021. **230**: p. 105-130.

20. Yang, X., et al., *Fuzzy adaptive singular value decomposition cubature Kalman filtering algorithm for lithium-ion battery state-of-charge estimation.* International Journal of Circuit Theory and Applications, 2021.

21. Liu, H., et al., *Comparisons on Kalman-Filter-Based Dynamic State Estimation Algorithms of Power Systems.* Ieee Access, 2020. **8**: p. 51035-51043.

22. Jiang, C., et al., *A state-of-charge estimation method of the power lithium-ion battery in complex conditions based on adaptive square root extended Kalman filter.* Energy, 2021. **219**: p. 256-287.

23. Duan, J.D., et al., *State of Charge Estimation of Lithium Battery Based on Improved Correntropy Extended Kalman Filter.* Energies, 2020. **13**(16): p. 557-598.

24. Zheng, T., et al., *SOC estimation of aging lithium battery based on adaptive CKF.* Energy Storage Science and Technology, 2020. **9**(4): p. 1193-1199.

25. Zhu, Q., et al., *A state of charge estimation method for lithium-ion batteries based on fractional order adaptive extended kalman filter.* Energy, 2019. **187**: p. 878-890.

26. Liu, Z., et al., *A State of Charge Estimation Method for Lithium-Ion Battery Using PID Compensator-Based Adaptive Extended Kalman Filter.* Complexity, 2021. **2021**: p. 1011-1101.

27. Agudelo, B.O., W. Zamboni, and E. Monmasson, *Application domain extension of incremental capacity-based battery SoH indicators.* Energy, 2021. **234**: p. 545-601.

28. Chang, C., et al., *Prognostics of the state of health for lithium-ion battery packs in energy storage applications.* Energy, 2022. **239**: p. 1200-1254.

29. Tran, M.K., et al., *A comprehensive equivalent circuit model for lithium-ion batteries, incorporating the effects of state of health, state of charge, and temperature on model parameters.* Journal of Energy Storage, 2021. **43**: p. 458-520.

30. Wu, J., et al., *Health Prognosis With Optimized Feature Selection for Lithium-Ion Battery in Electric Vehicle Applications.* Ieee Transactions on Power Electronics, 2021. **36**(11): p. 12646-12655.

31. Chang, C., et al., *Lithium-ion battery state of health estimation using the incremental capacity and wavelet neural networks with genetic algorithm.* Journal of Energy Storage, 2021. **38**: p. 566-600.

32. Hamar, J.C., et al., *State-of-health estimation using a neural network trained on vehicle data.* Journal of Power

Sources, 2021. **512**: p. 789-802.

33. Jia, J.F., et al., *A multi-scale state of health prediction framework of lithium-ion batteries considering the temperature variation during battery discharge.* Journal of Energy Storage, 2021. **42**: p. 447-480.

34. Bian, X.L., et al., *A Novel Model-Based Voltage Construction Method for Robust State-of-Health Estimation of Lithium-Ion Batteries.* Ieee Transactions on Industrial Electronics, 2021. **68**(12): p. 12173-12184.

35. Bian, X.L., et al., *State-of-Health Estimation of Lithium-Ion Batteries by Fusing an Open Circuit Voltage Model and Incremental Capacity Analysis.* Ieee Transactions on Power Electronics, 2022. **37**(2): p. 2226-2236.

36. Wang, J.H., et al., *Multiple Indicators-Based Health Diagnostics and Prognostics for Energy Storage Technologies Using Fuzzy Comprehensive Evaluation and Improved Multivariate Grey Model.* Ieee Transactions on Power Electronics, 2021. **36**(11): p. 12309-12320.

37. Gou, B., Y. Xu, and X. Feng, *An Ensemble Learning-Based Data-Driven Method for Online State-of-Health Estimation of Lithium-Ion Batteries.* Ieee Transactions on Transportation Electrification, 2021. **7**(2): p. 422-436.

38. Nagulapati, V.M., et al., *Capacity estimation of batteries: Influence of training dataset size and diversity on data driven prognostic models.* Reliability Engineering & System Safety, 2021. **216**: p. 665-740.

39. Zhang, J.A., et al., *SOH estimation of lithium-ion batteries based on least squares support vector machine error compensation model.* Journal of Power Electronics, 2021. **21**(11): p. 1712-1723.

40. Qian, K.F. and X.T. Liu, *Hybrid optimization strategy for lithium-ion battery's State of Charge/Health using joint of dual Kalman filter and Modified Sine-cosine Algorithm.* Journal of Energy Storage, 2021. **44**: p. 741-850.

41. Sui, X., et al., *A review of non-probabilistic machine learning-based state of health estimation techniques for Lithium-ion battery.* Applied Energy, 2021. **300**: p. 788-850.

42. An, Z., et al., *SOC estimation of lithium battery based on adaptive untracked Kalman filter.* Energy Storage Science and Technology, 2019. **8**(5): p. 856-861.

43. Ding, Z., et al., *SOC Estimation of Lithium-ion Battery Based on Ampere Hour Integral and Unscented Kalman Filter.* China Mechanical Engineering, 2020. **31**(15): p. 1823-1830.

44. Ye, P., et al., *Analysis and Identification on the Thevenin Equivalent Considering the Correlation of Source-grid-load.* Proceedings of the Chinese Society of Electrical Engineering, 2020. **40**(9): p. 2842-2853.

45. Guo, X., et al., *SOC Estimation with an Adaptive Unscented Kalman Filter Based on Model Parameter Optimization.* Applied Sciences-Basel, 2019. **9**(19): p. 784-820.

46. Guo, Y., Y. Dai, and S. Fu, *Estimation of battery SOC and SOH for urban rail vehicle composite power energy storage system.* Journal of Rail Way Science and Engineering, 2020. **17**(11): p. 2920-2928.

47. Lai, X., et al., *A comparative study of global optimization methods for parameter identification of different equivalent circuit models for Li-ion batteries.* Electrochimica Acta, 2019. **295**: p. 1057-1066.

48. Luo, Y., et al., *Second-order RC modeling and parameter identification of electric vehicle power battery.* Energy Storage Science and Technology, 2019. **8**(4): p. 738-744.

49. Sun, L., et al., *SOC estimation of Li-ion battery based on approximate second-order EKF.* Battery Bimonthly, 2019. **49**(5): p. 387-391.

50. Tian, M., et al., *SOC estimation of lithium battery based online parameter identification and AEKF.* Energy Storage Science and Technology, 2019. **8**(4): p. 745-750.

51. Wu, X. and X. Zhang, *Parameters identification of second order RC equivalent circuit model for lithium batteries.* Journal of Nanjing University. Natural Sciences, 2020. **56**(5): p. 754-761.

52. Xu, Y., et al., *State of Charge Estimation for Lithium-Ion Batteries Based on Temperature-Dependent Second-Order RC Model.* Electronics, 2019. **8**(9): p. 1424-1501.

Tab.1 Lithium-ion battery and BMS specifications

Battery type	Ternary lithium-ion battery		BMS type	BMS-HIL-1005
Size	149mm*98mm*40mm		Size	1800mm*700mm*1500mm
Standard capacity	70Ah		Input voltage	220V
Nominal voltage	3.7V		Max power	1500W
Internal resistance	5Ωm			
Maximum continuous discharge	3C			
Charging upper voltage	4.2V			
Discharge lower limit voltage	2.75V			

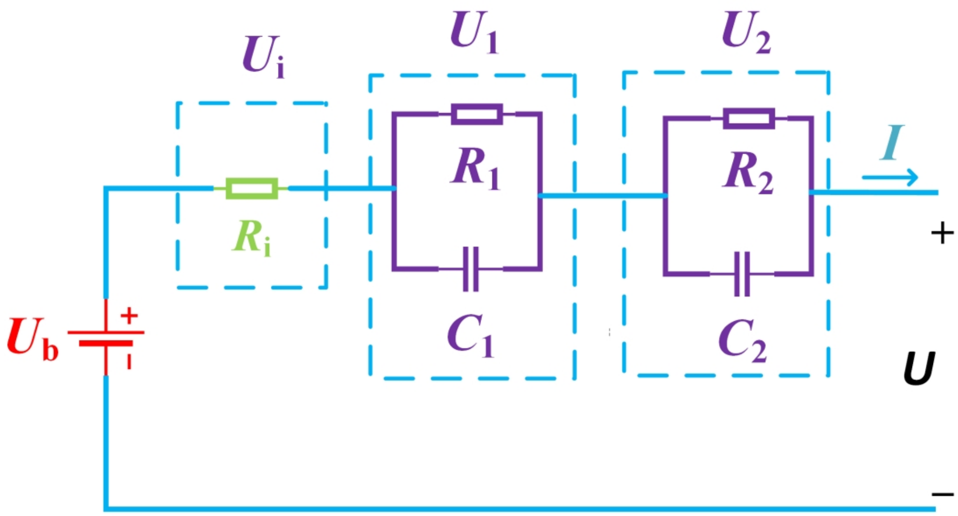

Fig. 1 Second order RC equivalent circuit model

201x107mm (300 x 300 DPI)

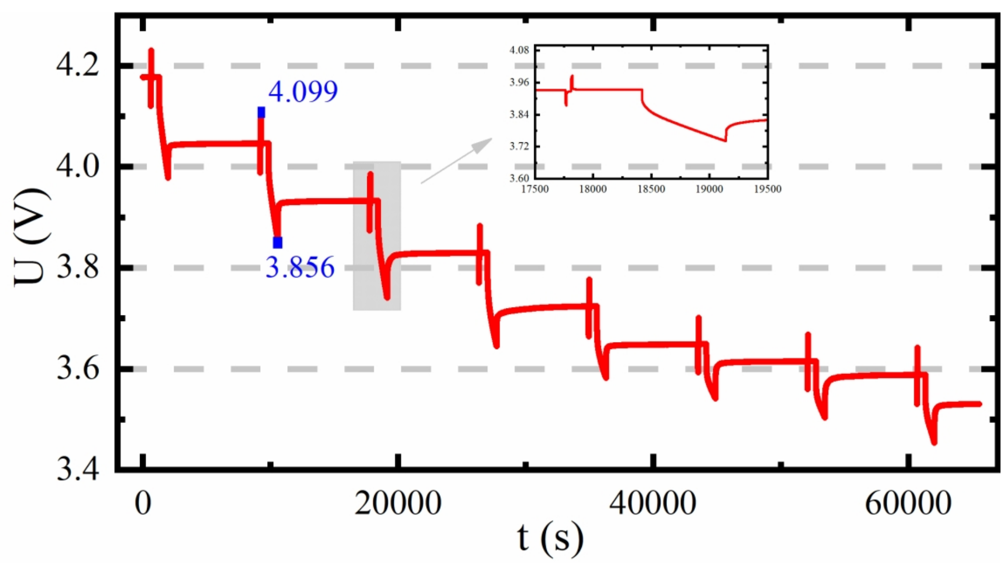

Fig. 2 (a) HPPC voltage curve

181x99mm (300 x 300 DPI)

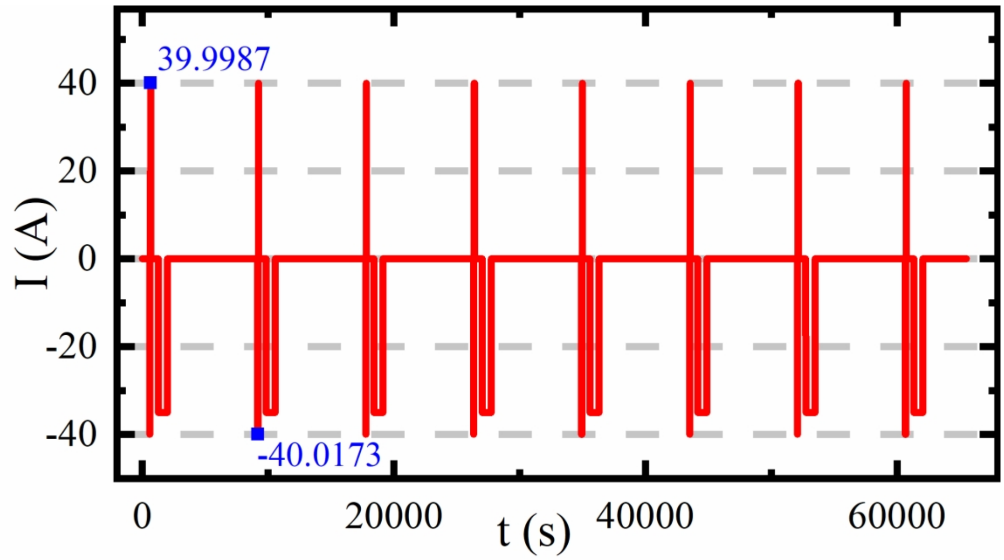

Fig. 2 (b) HPPC current curve

178x98mm (300 x 300 DPI)

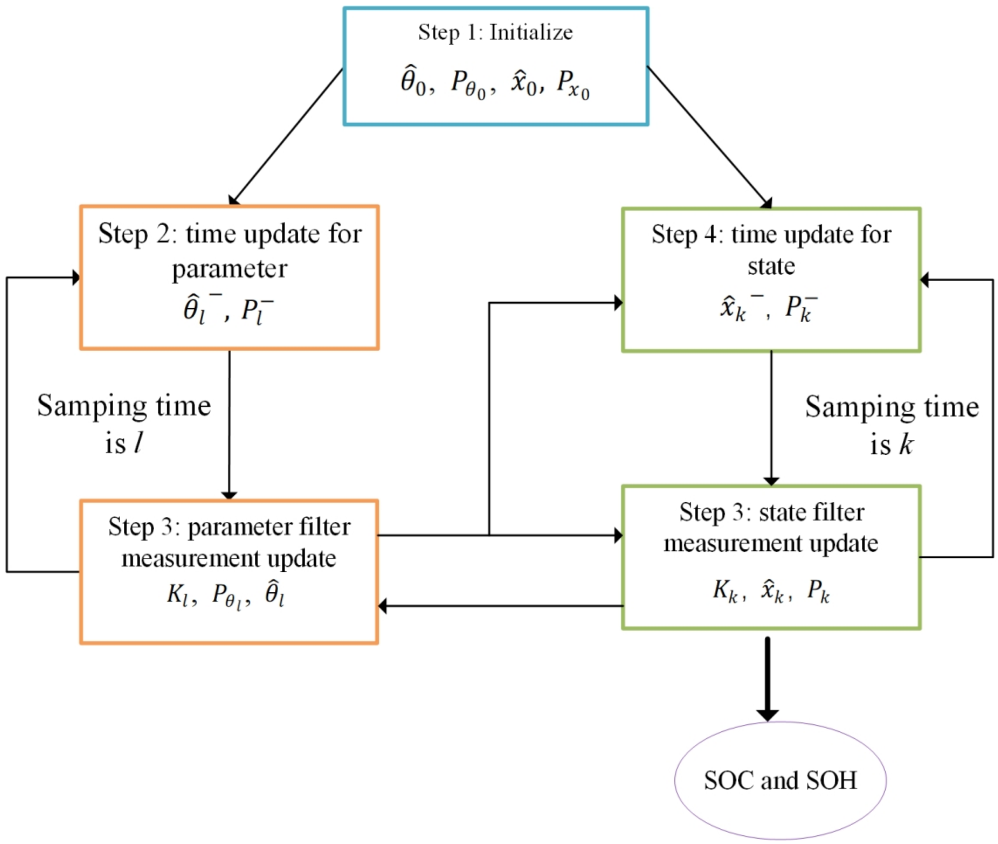

Fig.3 The flowchart of the multi time scale double extended Kalman filter

134x112mm (300 x 300 DPI)

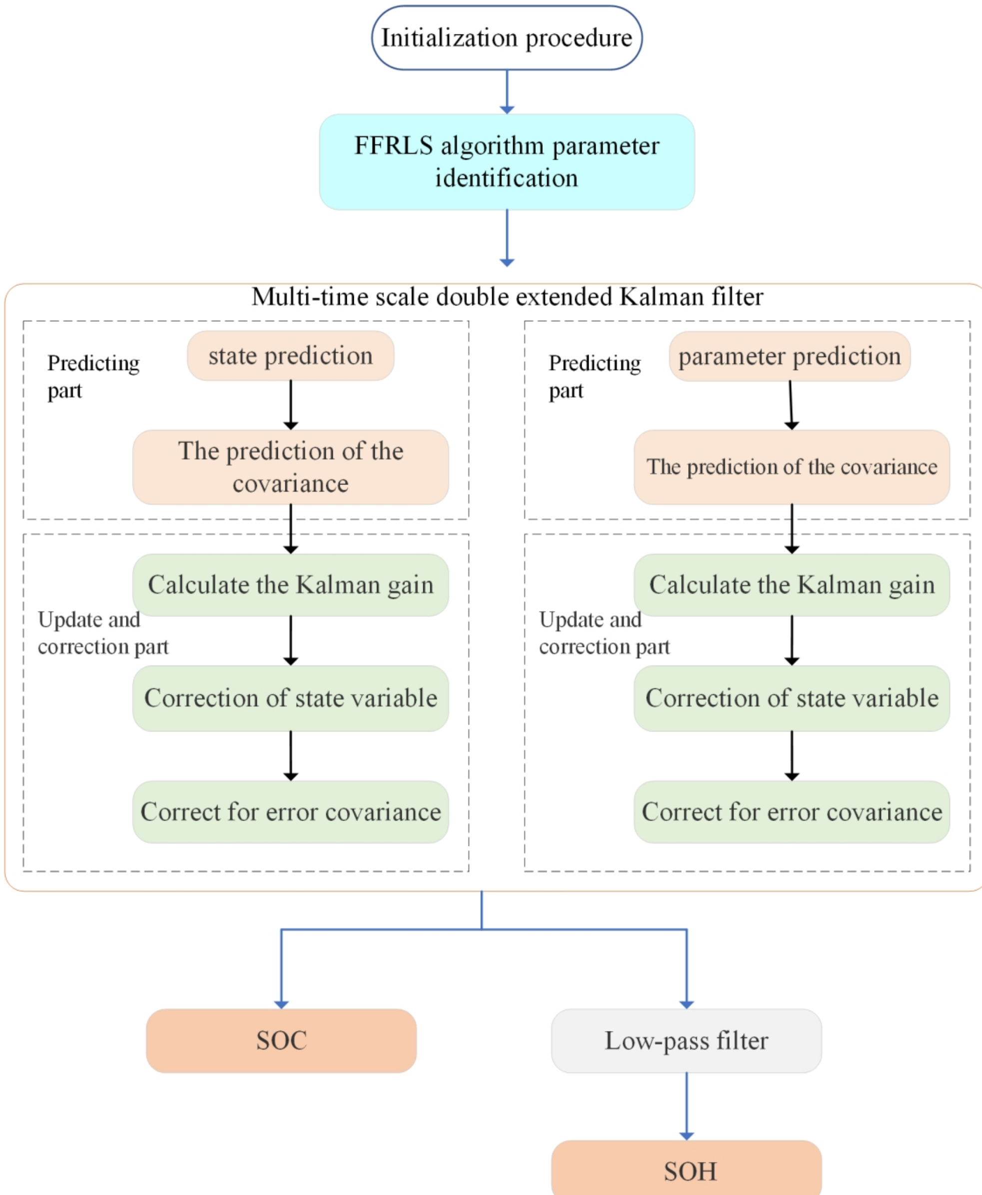

Fig.4 Flow chart of the multi-time scale low-pass filter FFRLS - DEKF algorithm

154x188mm (300 x 300 DPI)

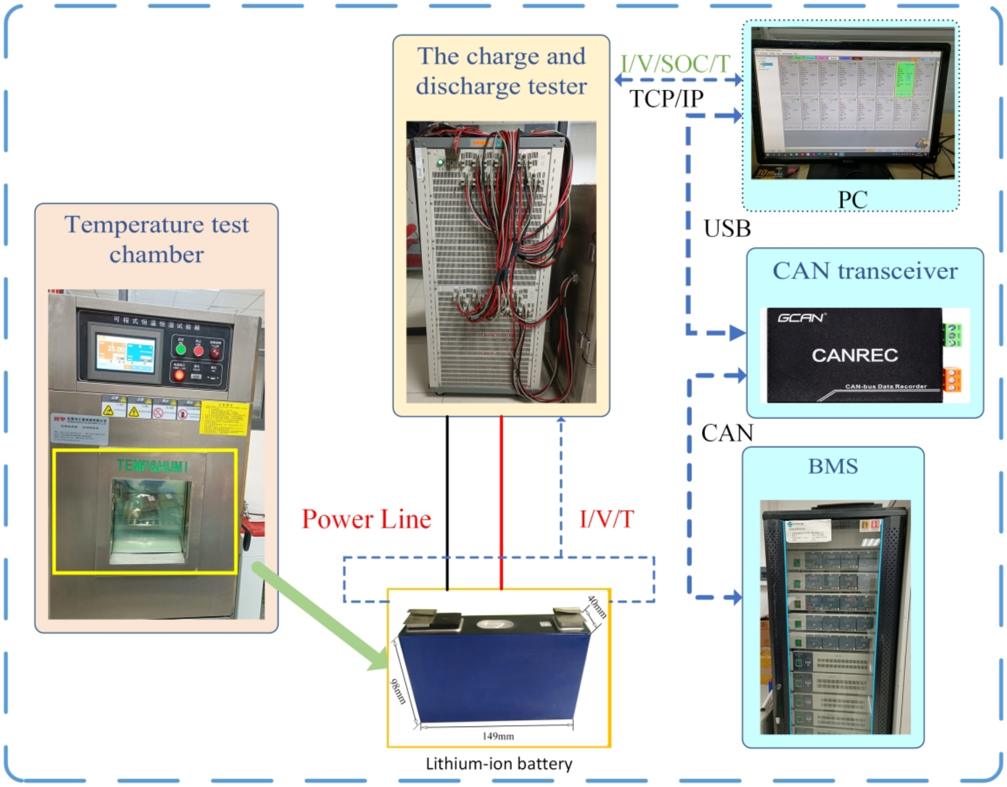

Fig.5 Experimental lithium-ion battery test platform

225x176mm (300 x 300 DPI)

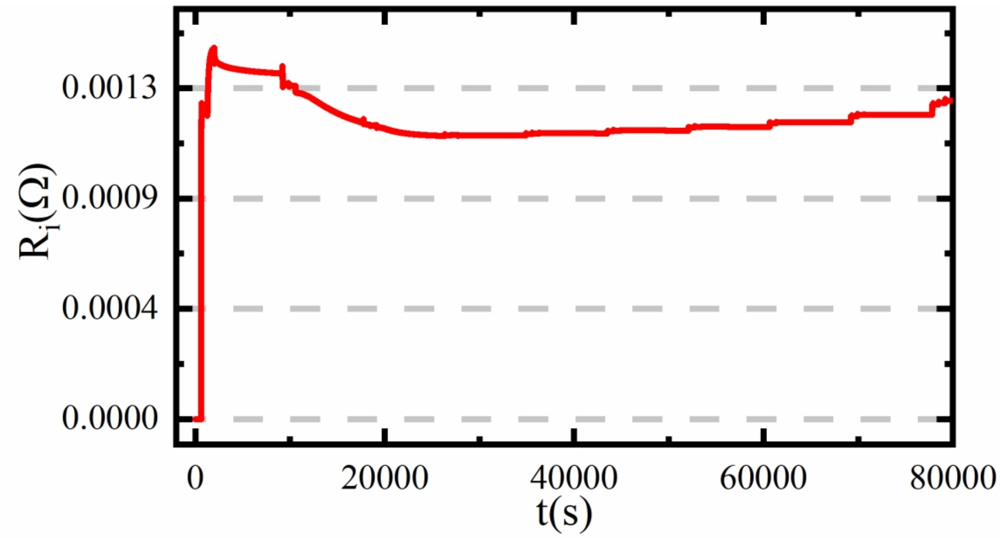

Fig. 6 (a) Ri identification result curve

180x96mm (300 x 300 DPI)

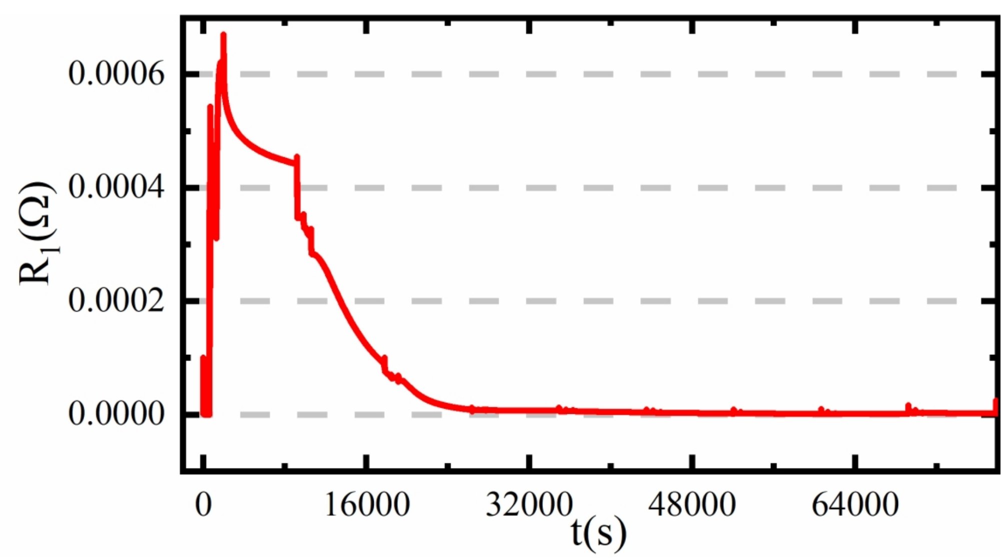

Fig. 6 (b) R1 identification result curve

179x97mm (300 x 300 DPI)

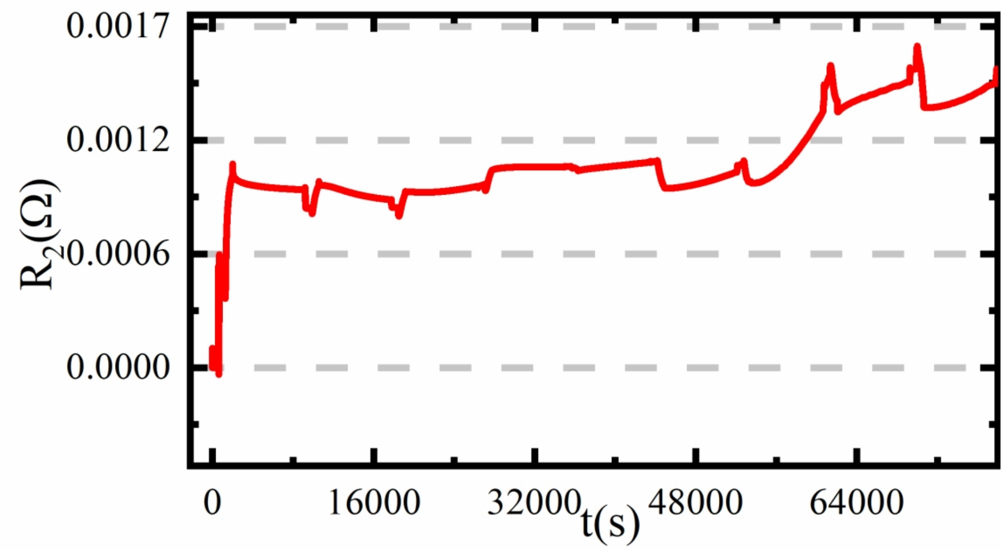

Fig. 6 (c) R2 identification result curve

183x100mm (300 x 300 DPI)

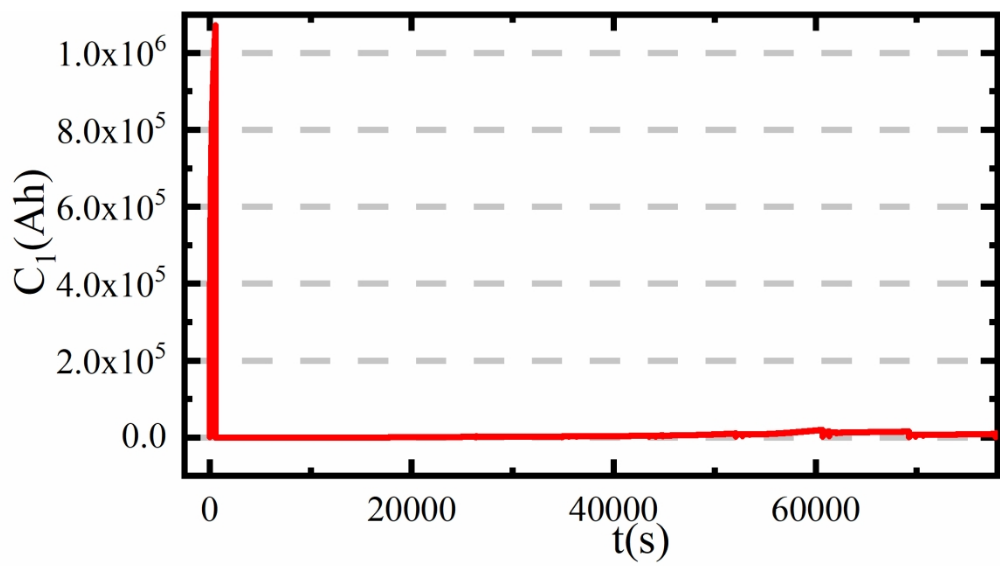

Fig. 6 (d) C1 identification result curve

177x98mm (300 x 300 DPI)

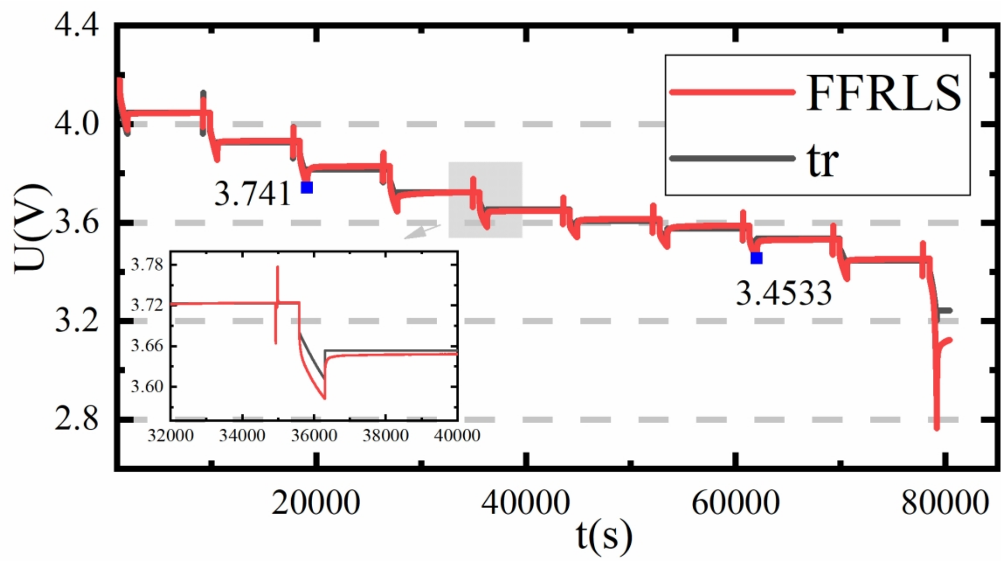

Fig. 7 (a) Comparison between simulated voltage and the actual voltage

177x99mm (300 x 300 DPI)

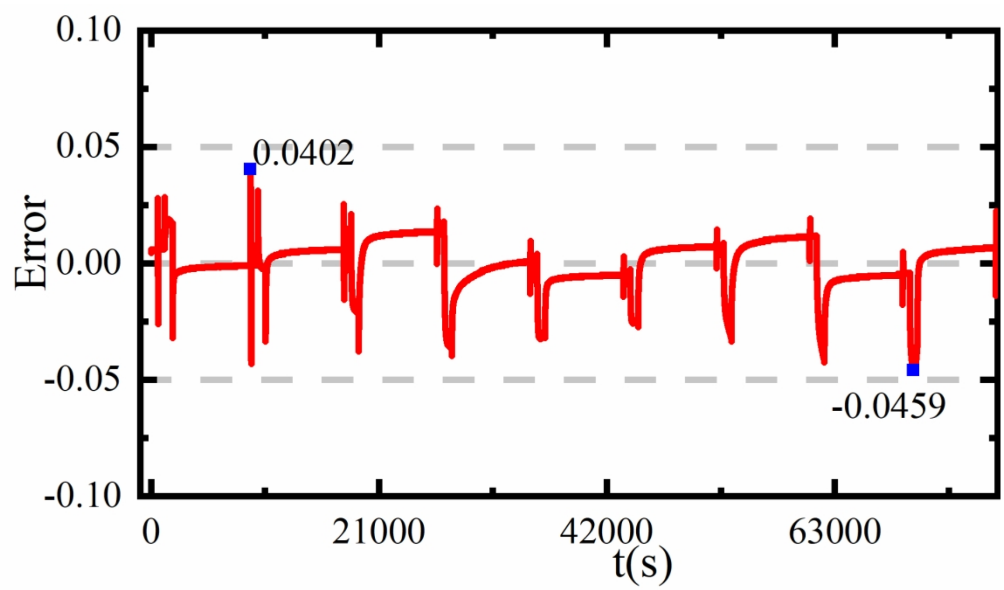

Fig. 7 (b) FFRLS simulation voltage error result curve

169x99mm (300 x 300 DPI)

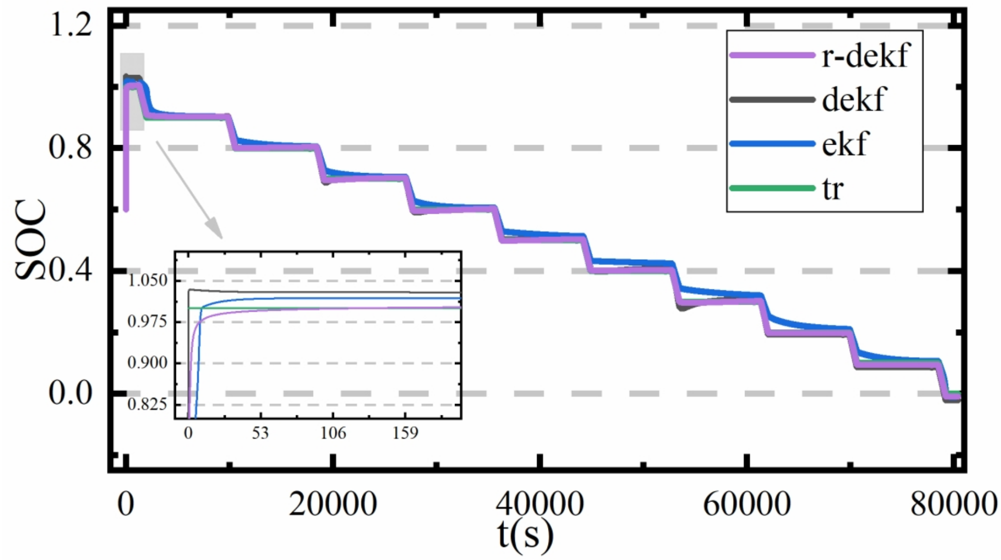

Fig. 8 (a) Estimated SOC and true SOC curve under HPPC condition

178x99mm (300 x 300 DPI)

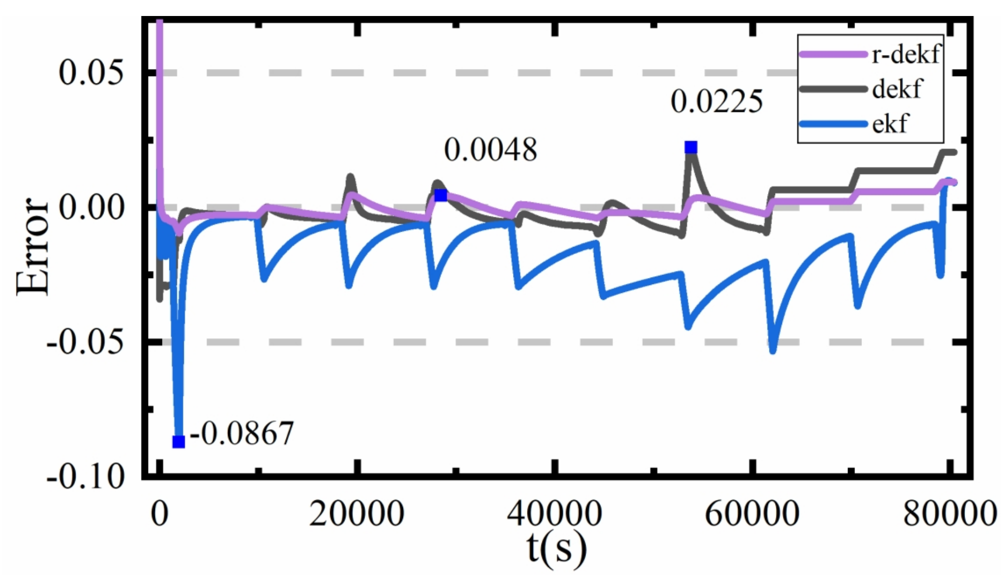

Fig. 8 (b) SOC error curve under HPPC condition

182x101mm (300 x 300 DPI)

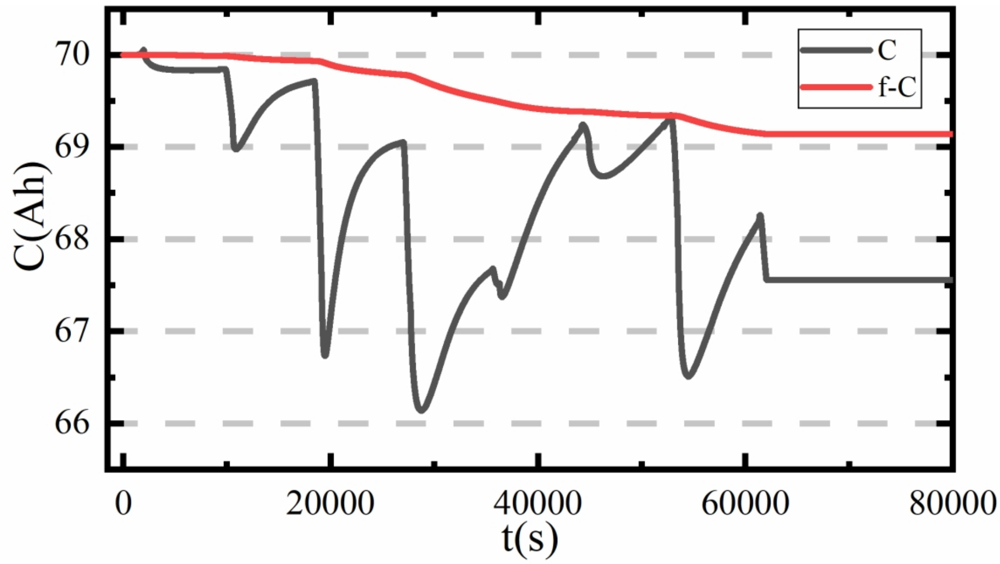

Fig. 8 (c) Estimated capacity and low-pass filter capacity under HPPC condition

178x99mm (300 x 300 DPI)

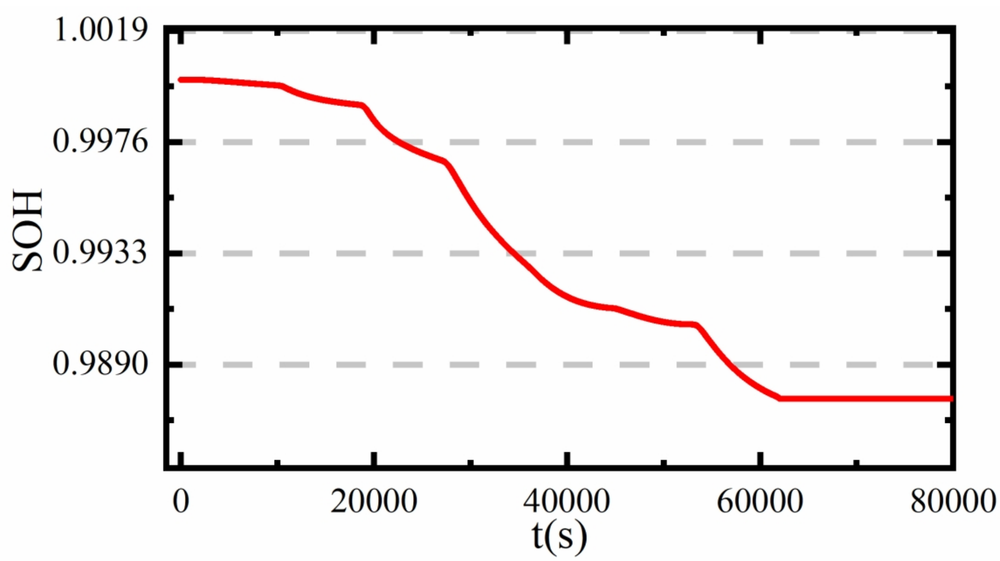

Fig. 8 (d) SOH curve under HPPC working condition

181x100mm (300 x 300 DPI)

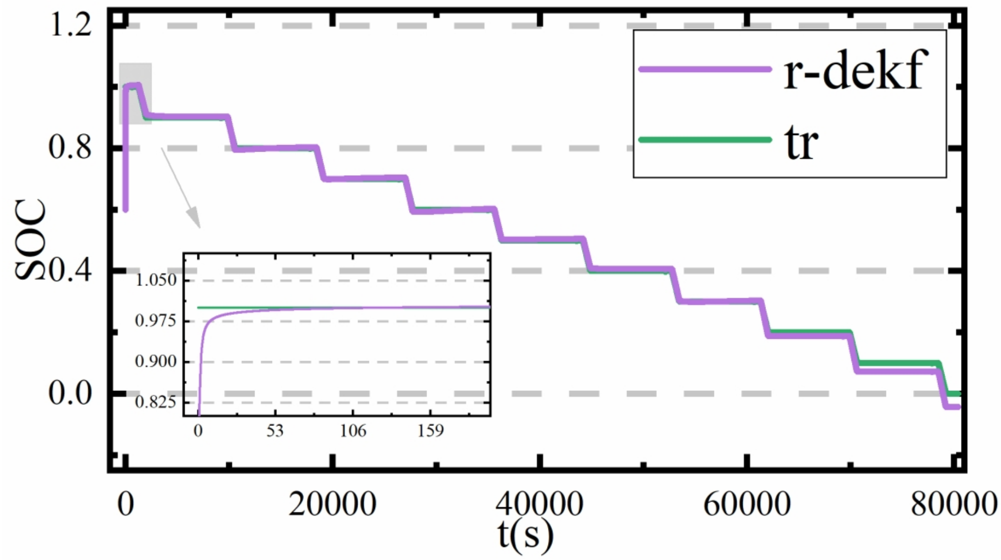

Fig. 9 (a) Estimated SOC and true SOC curve under HPPC condition

179x100mm (300 x 300 DPI)

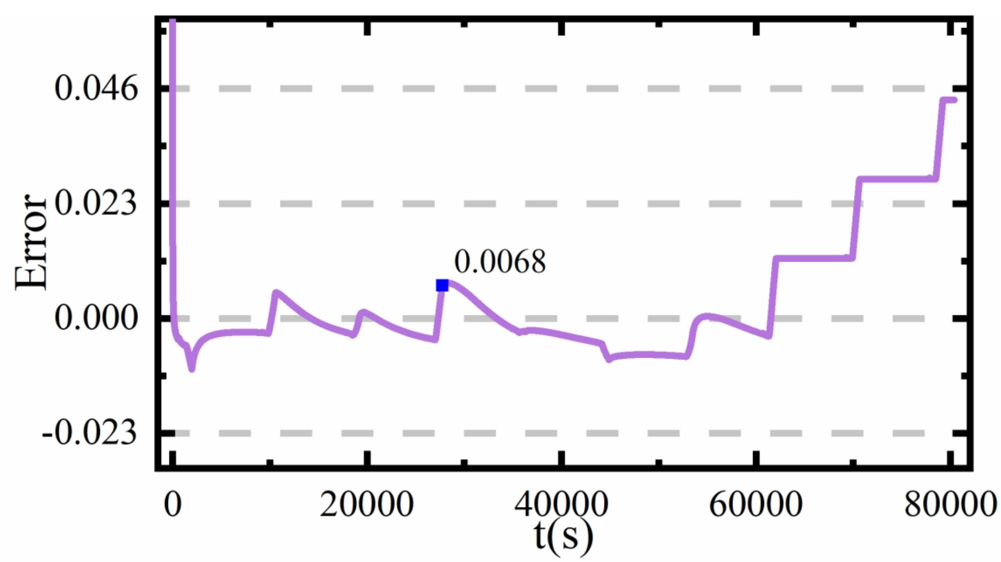

Fig. 9 (b) SOC error curve under HPPC condition

185x101mm (300 x 300 DPI)

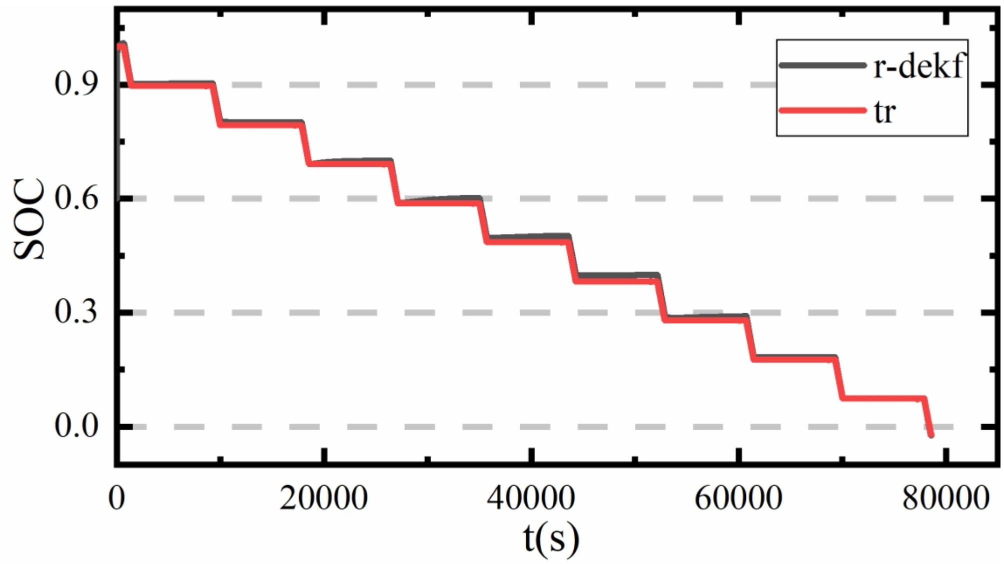

Fig.10 (a) Estimated SOC and true SOC curve under HPPC condition

178x99mm (300 x 300 DPI)

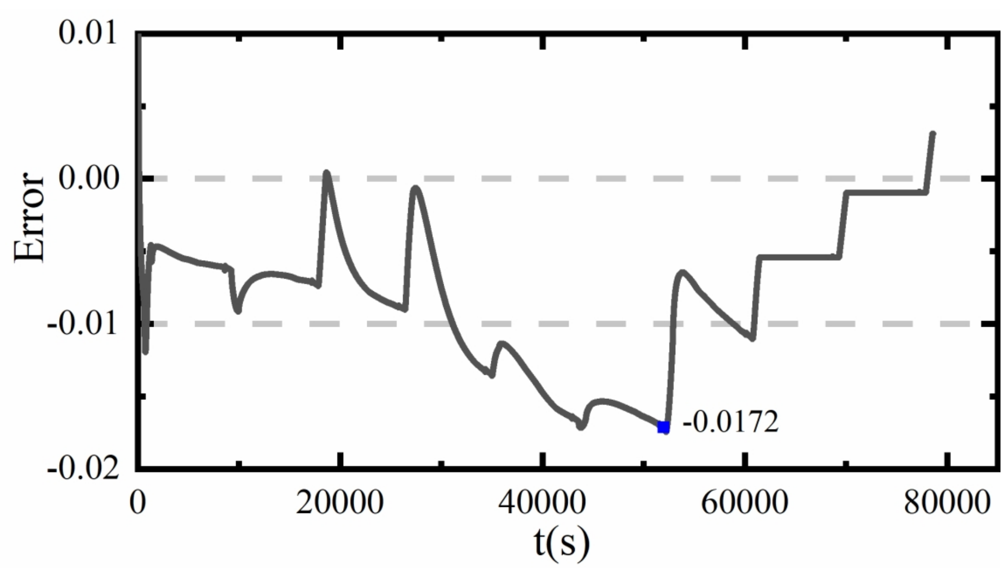

Fig.10 (b) SOC error curve under HPPC condition

179x100mm (300 x 300 DPI)

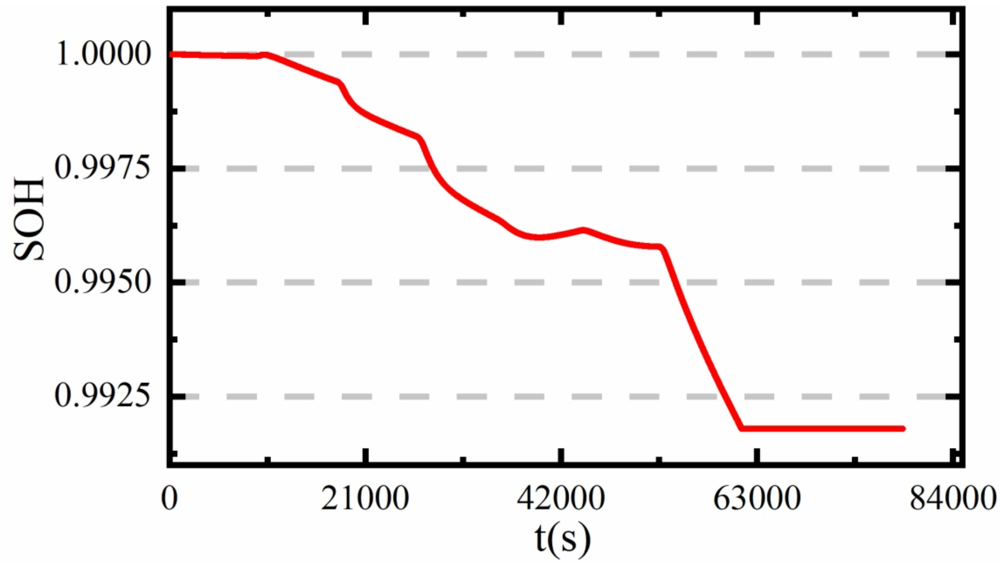

Fig.10 (c) SOH curve under HPPC working condition

178x100mm (300 x 300 DPI)

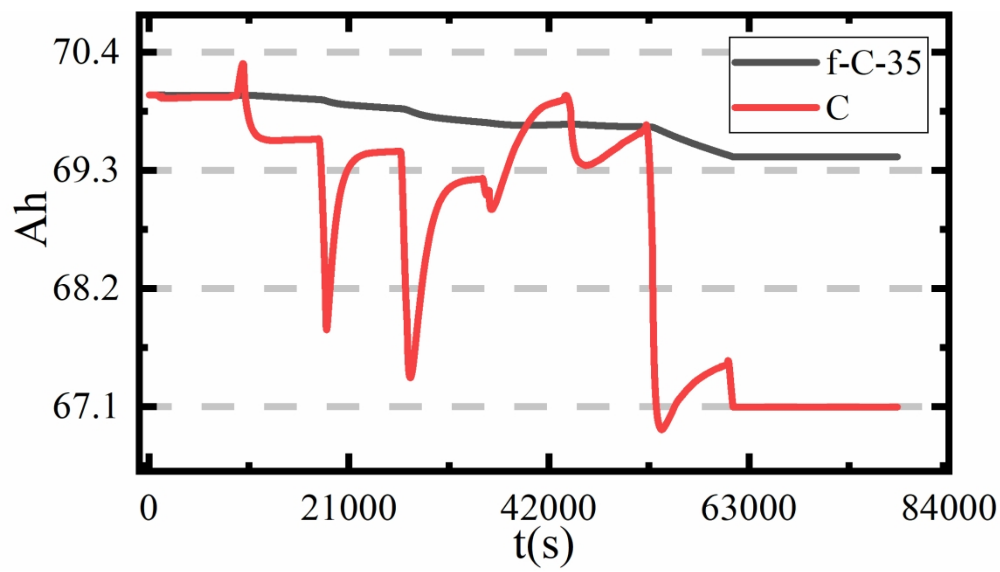

Fig.10 (d) Low-pass filtering effect

181x101mm (300 x 300 DPI)

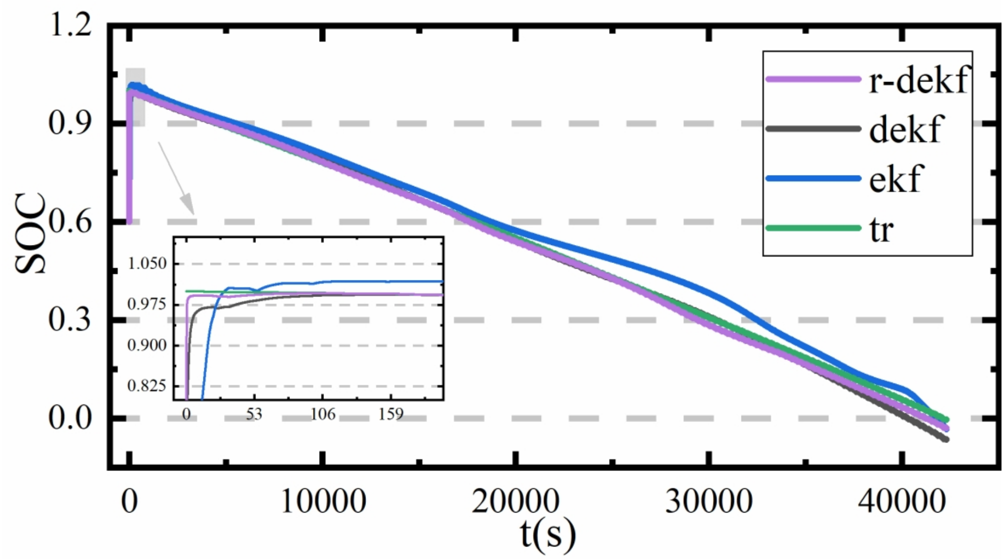

Fig. 11 (a) Estimated SOC and true SOC curve

179x100mm (300 x 300 DPI)

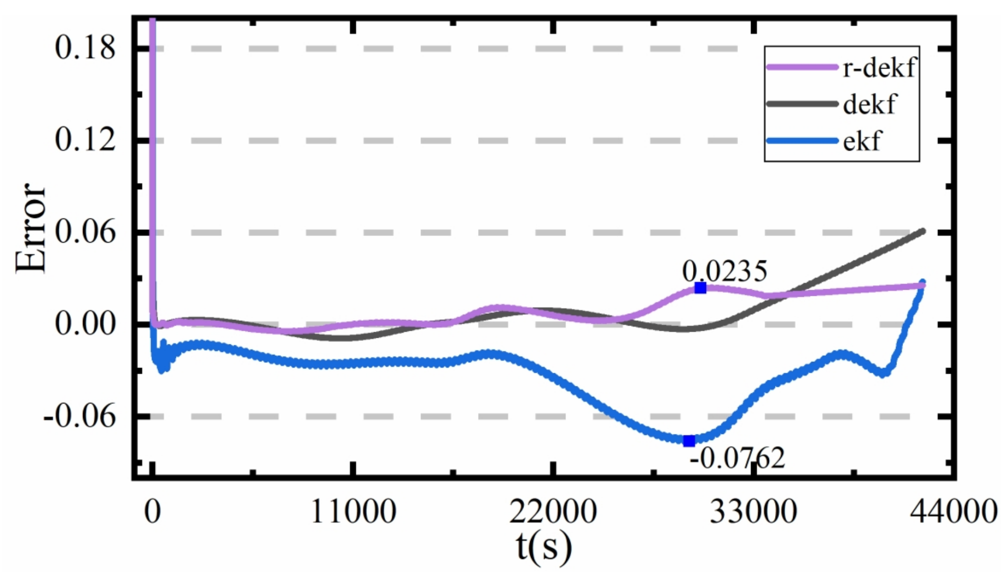

Fig. 11 (b) SOC error curve

179x99mm (300 x 300 DPI)

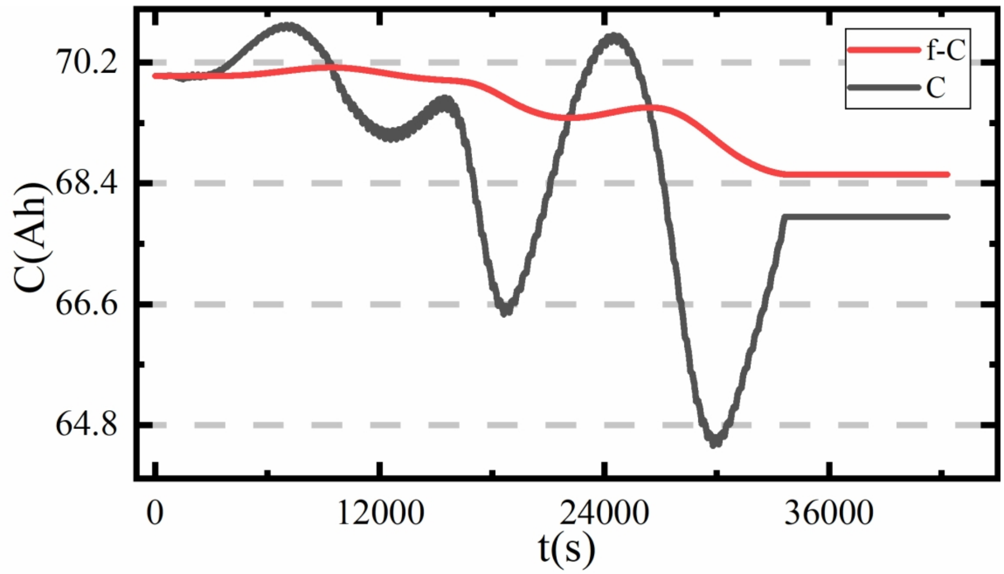

Fig. 11 (c) Estimated capacity and low-pass filter capacity diagram

175x100mm (300 x 300 DPI)

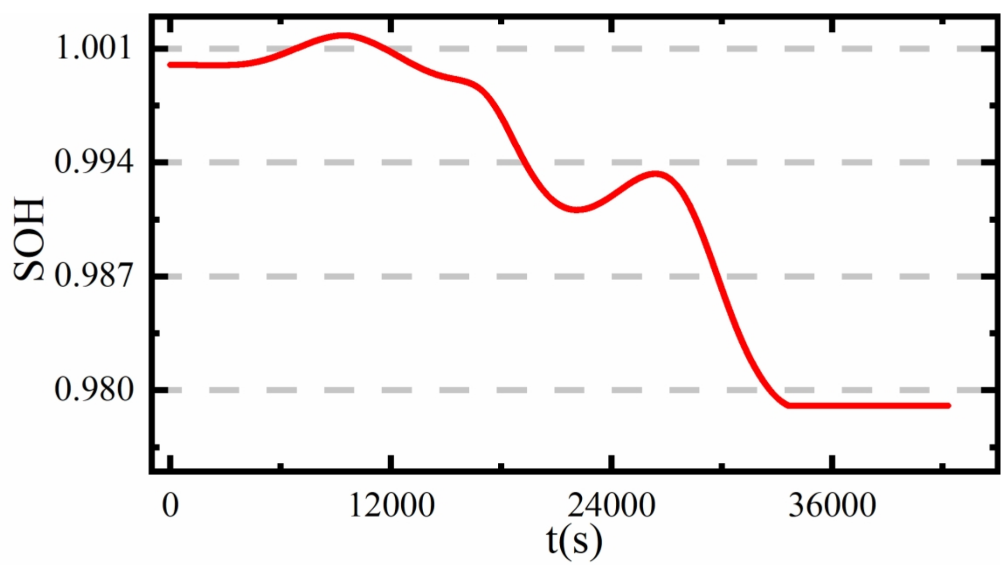

Fig. 11 (d) SOH curve

178x98mm (300 x 300 DPI)

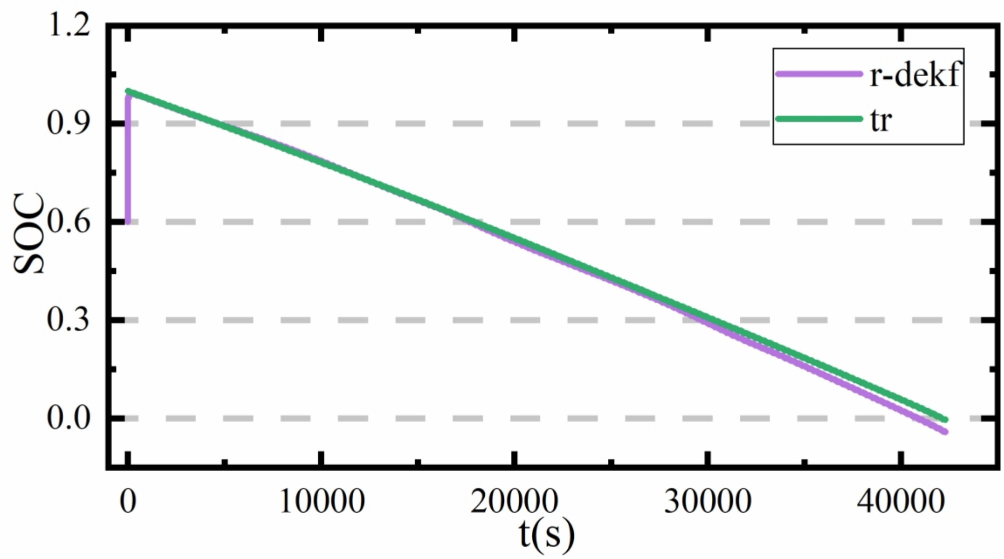

Fig. 12 (a) Estimated SOC and true SOC curve

179x100mm (300 x 300 DPI)

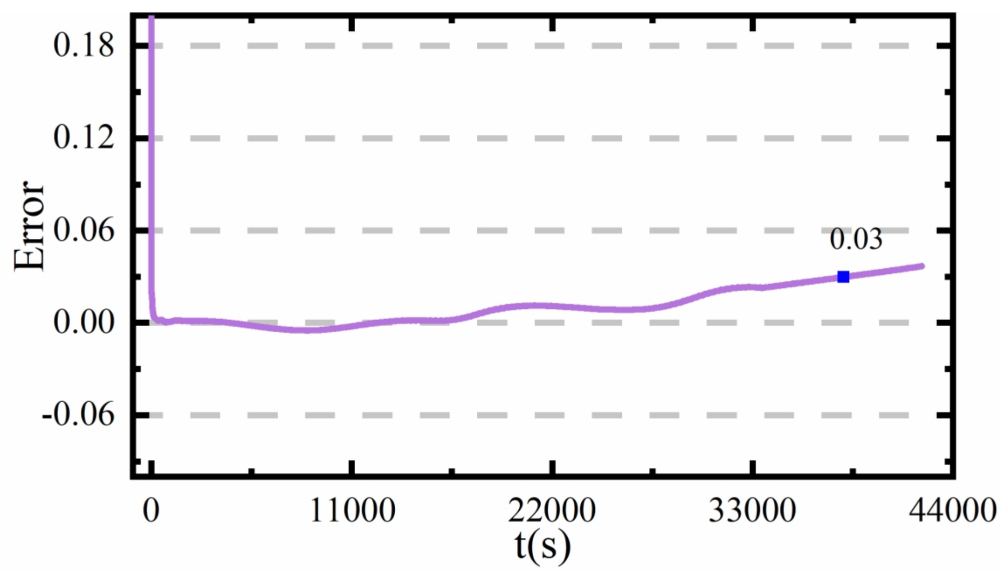

Fig. 12 (b) SOC error curve

179x100mm (300 x 300 DPI)

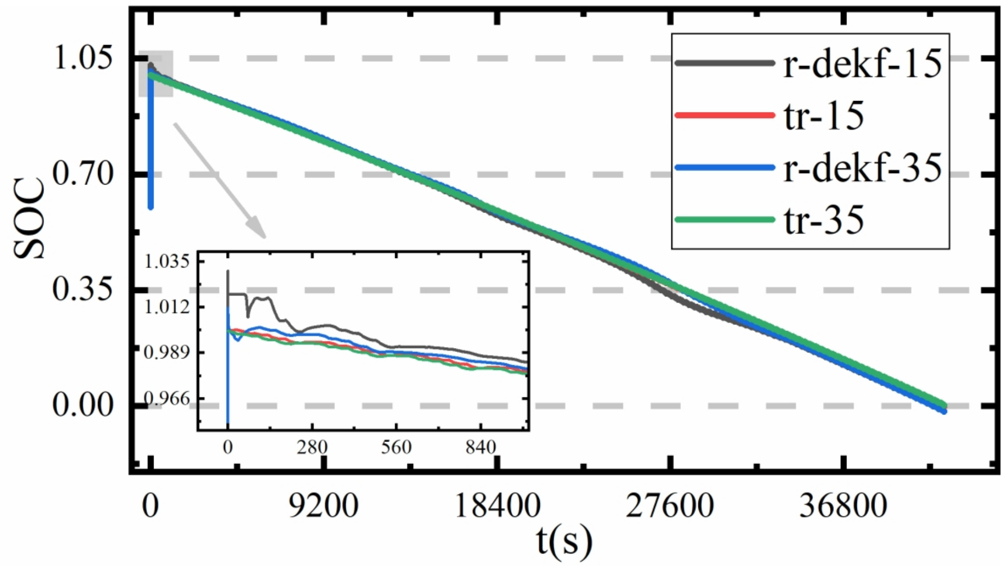

Fig.13 (a) Estimated SOC and true SOC curve

178x100mm (300 x 300 DPI)

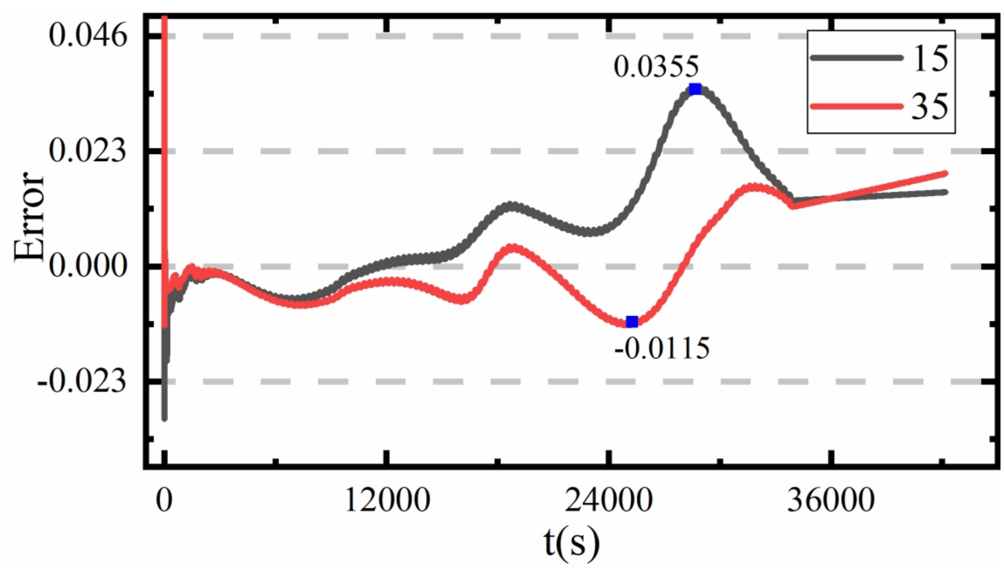

Fig.13 (b) SOC error curve

178x99mm (300 x 300 DPI)

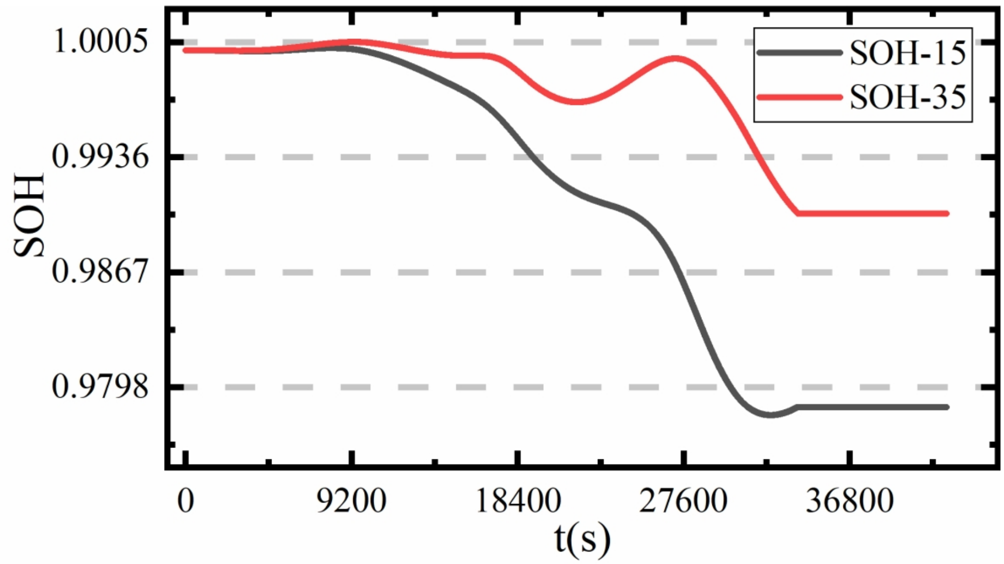

Fig.13 (c) SOH estimation curve

178x99mm (300 x 300 DPI)

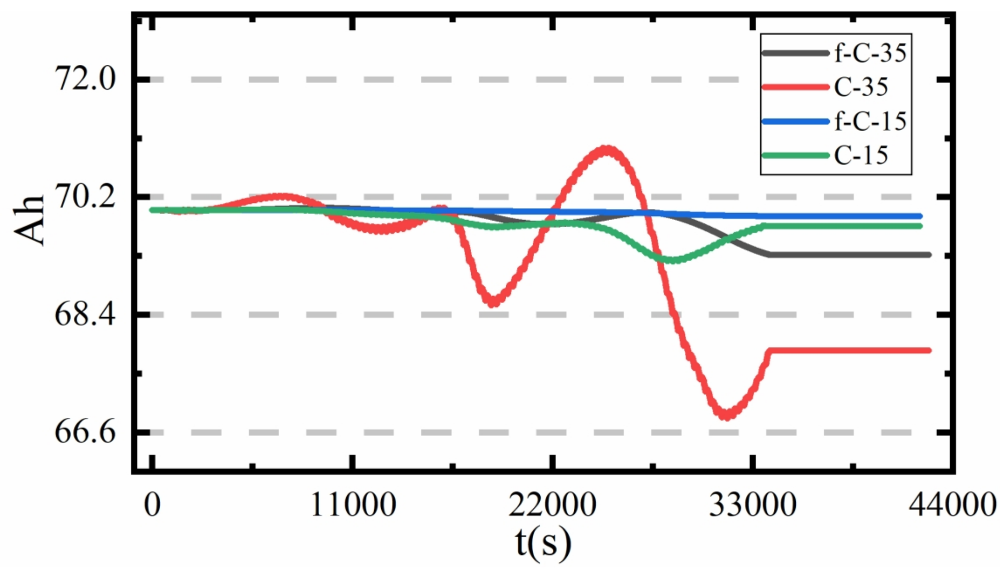

Fig.13 (d) Estimated capacity and low-pass filter capacity diagram

178x99mm (300 x 300 DPI)